gels

MDPI

Article

Construction of a Dynamic Covalently Modified Guar Gum Gel for High-Temperature Fracturing and Heavy-Oil Reservoir Stimulation

Qi Wang [1,2], Minghui Li [3,*], Jihong Zhang [1,*], Hailong Zhang [4] and Yiming Yang [5]

[1] Key Laboratory of Enhanced Oil and Gas Recovery, Northeast Petroleum University, Ministry of Education, Daqing 163318, China; 18945613366@163.com
[2] Daqing Oilfield Kaipu Chemical Co., Ltd., Daqing 163453, China
[3] Department of Geology, Qinhuangdao Campus, Northeast Petroleum University, Qinhuangdao 066004, China
[4] Daqing Oilfield Co., Ltd. Downhole Operations Branch, Daqing 163000, China; jx_zhanghl@petrochina.com.cn
[5] Liaohe Oilfield Exploration and Development Research Institute, CNPC, Panjin 124000, China; yangyiming521@126.com
* Correspondence: liminghui_0817@163.com (M.L.); dqzhjh@126.com (J.Z.)

Abstract

Fracturing ultra-deep reservoirs (>6000 m) at temperatures above 160 °C requires a gel that combines prolonged thermal stability, low formation damage, and controllable degradation; commercial guar-based fluids, such as hydroxypropyl guar crosslinked with organoboron, fail to meet this combination because of irreversible thermo-oxidative chain scission, as confirmed by our control experiments. In this study, a heat-resistant modified guar gum (GHPG) was used as the base polymer, and a dynamically crosslinked gel was constructed by optimizing the borate–ester crosslinking network. At 160 °C and 170 s^{-1}, the gel retained an apparent viscosity above 250 mPa·s after 120 min of continuous shear. At 180 °C without a breaker, it stayed above 80 mPa·s for 90 min. Upon triggering with 50 ppm ammonium persulfate at 180 °C, the network broke down within 70 min, reducing the viscosity below 10 mPa·s. This balance of long-term structural integrity and on-demand rapid breakage was achieved with a percolation-threshold-controlled network at an optimal crosslinker dosage of 0.6 vol%. Engineering evaluation gave a drag reduction rate of 58.02% (62 mm pipe, 6.0 m^3/min, fresh water baseline), a dynamic fluid-loss coefficient of 3.76×10^{-4} m/$min^{0.5}$, core-matrix damage of 16.2–18.5%, and fracture-conductivity damage of 14.64% at 85.0 MPa closure stress. A weighted variant (14 wt% NaCl) retained above 130 mPa·s after 2 h at 160 °C. The results establish a structure–property basis for gels in 160–180 °C ultra-deep fracturing. The low-residue, low-surface-tension, low-damage features also suggest potential application in heavy-oil fracturing; dedicated crude-compatibility and emulsification tests remain required before field deployment.

Keywords: high-temperature fracturing fluid; modified guar gum gel; reversible crosslinked network; crosslinker concentration threshold; drag reduction; formation damage; heavy-oil stimulation; low-damage flowback

Check for updates

Academic Editor: Georgios Bokias

Received: 30 October 2026
Revised: 20 November 2026
Accepted: 21 November 2026
Published: 25 November 2026

Copyright: © 2026 by the authors. Licensee MDPI, Basel, Switzerland. This article is an open access article distributed under the terms and conditions of the Creative Commons Attribution (CC BY) license.

1. Introduction

As global hydrocarbon exploration extends progressively into deep and ultra-deep formations (burial depth > 6000 m), reservoir temperatures have surpassed 160 °C and, in certain well blocks, exceed 200 °C, thereby placing high demands on the high-temperature rheological behavior and formation-protection capacity of fracturing fluids [1–4]. The

Tarim Basin and Sichuan Basin in China contain abundant deep resources; for instance, the peripheral Tahe Oilfield exhibits reservoir temperatures of 160–180 °C. Under such extreme conditions, conventional guar-gum fracturing fluids undergo irreversible thermal degradation, rapidly losing viscosity and failing to transport proppant and generate fractures. Constructing a gel network that maintains structural integrity over extended periods at temperatures above 160 °C has therefore emerged as a key scientific challenge for the efficient development of deep hydrocarbon resources. At the same time, heavy-oil reservoirs, commonly characterized by high in situ crude viscosity, low matrix permeability, strong water sensitivity, and difficult post-treatment flowback, rely on proppant-supported fractures to achieve commercial production; residual polymer and filter-cake damage in such intervals can substantially erode the productivity gain delivered by the created fracture [5–7].

The cornerstone of water-based fracturing fluids is the thickener. Guar gum and its derivatives are widely used owing to their low cost and high thickening efficiency; however, the glycosidic bonds on the molecular backbone are susceptible to thermo-oxidative scission at elevated temperatures, restricting the practical service limit of unmodified guar to approximately 150 °C [1,8–10]. Chemical modification of guar gum is therefore regarded as the primary strategy for overcoming this temperature barrier. Zhang et al. (2022) comprehensively reviewed the development trends of high-temperature-resistant guar gum fracturing fluids, identifying the temperature-tolerant modification of guar and the synthesis of novel high-temperature-resistant crosslinkers as the two central directions for advancement [1]. Jing et al. (2018) synthesized a modified hydroxypropyl guar gum whose thermal degradation temperature was elevated above 220 °C [8].

Beyond biopolymer modification, substantial progress has been achieved in the design of synthetic polymers. Li et al. (2025) reported a hydrophobically associating polymer fracturing fluid that retained favorable rheological properties at 200 °C and 45 g/L NaCl, broadening the application envelope of synthetic polymers in high-temperature reservoirs [9]. Du et al. (2022) provided a systematic review of water-soluble polymers for high-temperature hydraulic fracturing, establishing a clear structure–property relationship: high molecular weight, extensive intermolecular association via hydrogen bonding, and the use of high-temperature-resistant additives (organometallic crosslinkers and gel stabilizers) enable biopolymer-based fluids to withstand environments below 150 °C, whereas synthetic polymers with C–C covalent backbones and functional side-chain groups can achieve temperature tolerance up to 240 °C [10]. Barati and Liang (2014) reviewed the design principles of high-temperature fracturing fluids, emphasizing the critical role of crosslinker chemistry in maintaining viscosity under extreme thermal conditions [11]. Moreover, Almubarak et al. (2021) systematically evaluated the thermal stability of various guar derivatives and identified the degradation kinetics as a key limiting factor for field applications above 150 °C [12].

At the level of crosslinking chemistry, the choice of crosslinker governs the thermal stability and dynamic reversibility of the gel network. Organoborate crosslinkers, which possess delayed crosslinking characteristics, have been widely applied in guar-based fracturing fluids since the 1990s to enhance viscoelasticity and proppant transport while avoiding premature viscosity buildup in the tubing [1,10]. Single organoborate systems, however, still lack sufficient thermal stability above 180 °C; transition-metal crosslinkers such as organozirconate and organotitanate offer superior temperature resistance but suffer from excessively rapid crosslinking and high residue contents after gel breaking. Yang et al. (2019) developed an organic borate–zirconium composite crosslinker in an attempt to combine the advantages of delayed crosslinking and high-temperature stability [13]. In recent years, nano-crosslinking technology has emerged as a promising frontier. Zhang et al. (2023) synthesized a boron-functionalized nanosilica colloidal crosslinker that, through the

synergistic effect of hydrogen and covalent bonding with guar gum molecules, enhanced the temperature resistance of hydroxypropyl guar gum (HPG) fracturing fluid by 7–18 °C and shear resistance by 5–20 mPa·s compared with conventional organoboron crosslinkers [14]. Zhang et al. (2022) further proposed that nano-crosslinked fracturing fluids with high efficiency and low damage represent a potential future development direction [1]. More recently, Ma et al. (2023) published a study in Gels on the development and gelation mechanism of an ultra-high-temperature-resistant polymer gel, demonstrating that a synthesized temperature-resistant polymer crosslinked with an organic zirconium agent retained a viscosity of 147 mPa·s at 200 °C and 170 s^{-1}, with a core damage rate of only 16.6% [15].

The field of supramolecular polymers has also attracted attention for high-temperature fracturing fluid applications. Zuo et al. (2025) reviewed the supramolecular polymers used in high-temperature fracturing fluids from the perspective of the coupling relationship between molecular conformation and temperature-resistance mechanisms [16]. Wang et al. (2024) systematically reviewed supramolecular fracturing fluids based on hydrophobic association, hydrogen bonding, electrostatic interaction, and host–guest inclusion, noting that while these self-assembled systems exhibit shear reversibility and adaptive characteristics, their widespread application remains constrained by poor temperature and salt resistance, harsh operating conditions, and high cost [17]. Most recently, Huang et al. (2024) published a study in Gels on a supramolecular reinforced gel (SRG) fracturing fluid, demonstrating that by strengthening supramolecular forces between polymers, an SRG with high elasticity ($G' = 12.20$ Pa) could be achieved at ultralow polymer (0.4 wt%) and crosslinker (0.1 wt%) concentrations [18].

More broadly, the architecture and dynamics of crosslinked hydrogel networks govern their viscoelastic response and long-term integrity. Reversible chemical linkages with tunable stress relaxation illustrate how junction lifetime controls network viscoelasticity [19]. Network heterogeneity—spatial variation in crosslink density and strand length—can decouple microscopic and macroscopic elasticity, and is typically resolved by scattering or force microscopy rather than by rheology or FTIR alone [20]. These perspectives frame the present interpretation of the borate–ester junction network in the fracturing gel.

Beyond thermal stability, the engineering service performance of fracturing fluids—encompassing drag reduction, fluid-loss control, and formation protection—directly determines operational safety and stimulation efficacy. The turbulent frictional resistance along the tubing is the principal factor affecting wellhead pressure; studies have demonstrated that optimizing polymer molecular weight and hydrodynamic volume in solution can substantially reduce pipe-flow friction [3,4]. The fluid-loss characteristics of fracturing fluids directly influence fracture dimensions and fluid efficiency. Liu et al. (2014) investigated the damage characteristics of guar-gum fracturing fluids to reservoirs, demonstrating that gel-breaking residues constitute the primary cause of impairment to both proppant-pack conductivity and matrix permeability, and that residue damage can persist even at low apparent viscosity [21]. Guo and He (2012) further elucidated the microscopic mechanism of damage during the gelout process, showing that polymer residues arising from incomplete gel breaking are a major cause of conductivity impairment, and that conventional viscosity-based criteria for judging gel breaking are insufficient [22]. Wang et al. (2020) studied gel-breaking performance and fracture conductivity damage under high-temperature and high-pressure conditions, revealing that the detrimental effects of gel breaker residue are amplified at high closure pressures above 50 MPa [23].

For deep, high-pressure reservoirs, increasing the fracturing-fluid density can augment hydrostatic pressure and thus reduce wellhead operating pressure. NaCl and NaBr are among the commonly employed weighting agents. Wu et al. (2011) investigated the effect of NaCl and NaBr on the weighting performance of high-temperature guar gum fractur-

ing fluid, demonstrating that salt content exhibits a well-defined relationship with fluid density and high-temperature rheology [24]. The weighting strategy, however, introduces additional complexity in maintaining crosslinker compatibility and high-temperature rheological stability. In the broader context of deep reservoir stimulation, Lei et al. (2021) reviewed the development history of stimulation techniques for ultra-deep oil and gas reservoirs, concluding that the requirements for fracturing materials in deep stimulation are exceptionally demanding, and that developing high-efficiency fracturing materials remains a critical technical direction [25]. Furthermore, the environmental dimension of fracturing fluid management has gained increasing prominence. Tan et al. (2023) reviewed the removal of organic pollutants from shale gas fracturing flowback and produced water, highlighting that effective management of fracturing fluid residues throughout the operational lifecycle—from injection to flowback—constitutes an integral component of sustainable reservoir development, and that integrated coagulation–sorption–Fenton–membrane filtration represents a promising treatment process [26].

Although heavy-oil development has traditionally relied on thermal recovery processes such as cyclic steam stimulation and steam-assisted gravity drainage [6], hydraulic fracturing remains a necessary stimulation route for low-permeability, deep or glutenite heavy-oil intervals where natural energy and steam injection alone cannot establish economic production [5]. The fluid-service requirements for these intervals overlap closely with those of high-temperature deep reservoirs: sustained viscosity for proppant transport, controlled fluid loss, thorough gel breaking with low residue, low surface and interfacial tension to promote flowback, and compatibility with high-salinity formation water. Field practice in the Tuha ultra-low-permeability glutenite heavy-oil reservoirs (3600–4800 m, 100–120 °C, crude viscosity 111.3–24,570 mPa·s at 50 °C) indicated that a low-concentration, low-damage crosslinked guar system reduced matrix damage by approximately 10% and improved fracture conductivity by about 15% relative to a conventional 0.45 wt% HPG fluid [5], confirming that thermal stability, low residue and conductivity protection—the central metrics of the present study—are equally decisive for heavy-oil stimulation.

In summary, although substantial progress has been made in the field of high-temperature fracturing fluids, the following core scientific and engineering challenges remain: (1) a fundamental contradiction persists between the long-term network stability required for proppant transport and the rapid, complete degradation demanded for formation protection; (2) commercial HPG–borate systems exhibit rapid viscosity decay at temperatures above 150 °C (demonstrated in Section 2.4.3), and existing synthetic polymer gels often compromise formation protection; (3) the role of crosslinking density—in particular, the threshold concentration governing the transition from a transient, shear-vulnerable network to a stable cooperative network under extreme conditions—has not been quantitatively elucidated; and (4) systematic research on the maintenance of high-temperature rheology and crosslinker compatibility in weighted systems remains lacking. In addition, a fifth gap concerns the transfer of a high-performance, low-damage gel formulation to heavy-oil reservoirs: compatibility with viscous crude, emulsion tendency and coupling with thermal-recovery conditions have not been systematically investigated [5,6].

To address these gaps, this study introduces three distinct innovations beyond prior reports on modified guar or borate-crosslinked gels:

The distinction from previously reported borate-crosslinked guar systems should be stated explicitly. Conventional organoborate HPG–guar gels rely on discrete, stoichiometric borate–cis-diol coordination between borate ions and the vicinal hydroxyls of guar side chains; these coordination bonds exchange rapidly under alkaline conditions but are thermally labile above roughly 140–150 °C, and the unmodified glycosidic backbone still undergoes irreversible thermo-oxidative scission, so that once a junction dissociates at high

temperature it is not restored, and viscosity decays rapidly [1,10,12]. The present system differs in three respects. First, the GHPG backbone is chemically modified with rigid hydroxypropyl and carboxymethyl groups that raise the chain-level degradation temperature. Second, the organoborate crosslinker carries an organic ligand (triethanolamine) that moderates boron release and junction dynamics, so that the borate–ester junctions are arranged as a system-spanning, cooperative network rather than isolated transient crosslinks. Third, the formulation is operated at a quantitatively identified threshold concentration (0.6 vol%), where a percolation transition from a viscous fluid ($G'' > G'$) to an elastic gel ($G' > G''$ plateau) occurs; together with a thiourea-derived radical scavenger, this dense junction network slows network disintegration and suppresses thermo-oxidative chain scission under high-temperature shear. The crosslinker dosage in this formulation was therefore selected from a mapped rheological transition rather than by empirical trial.

(i) Identification of a crosslinker-concentration threshold (0.6 vol%). As opposed to empirical optimization in commercial formulations, the rheological transition from a viscous fluid ($G'' > G'$) to an elastic gel ($G' > G''$ plateau) was mapped with frequency sweep and thixotropic recovery tests, and the observed transition is interpreted as a percolation-like network formation.

(ii) A dual-function system achieving both long-term thermal stability (>250 mPa·s for 120 min at 160 °C) and on-demand rapid breakage (<10 mPa·s within 70 min at 180 °C). Commercial HPG–borate fluids lose viscosity to <100 mPa·s within 60 min at 160 °C (Section 2.4.3) and require longer break times under the same conditions; the present gel combines sustained shear stability with controlled, triggered degradation.

(iii) Engineering validation under high closure stress (85 MPa) and high-salinity formation water, with direct comparison to literature benchmarks and one commercial control. The measured matrix damage was <19% and conductivity damage < 15% on the cores and fluids tested.

Beyond the specific chemistry of fracturing fluids, the broader context of reservoir geomechanics and stimulation efficiency has also been explored in recent studies. For instance, Wang et al. [27] investigated the influence of native pores on rock failure predictability, and Lei et al. [28] developed a semi-analytical model for hydraulically fractured horizontal wells in shale reservoirs. While these works address different aspects of reservoir stimulation, they underscore the need for integrated approaches combining advanced materials and predictive modeling.

Accordingly, the present study employs GHPG as the matrix to construct a gel system that exhibits high-temperature resistance, low formation damage, and controllable behavior. Through optimization of the crosslinked network architecture, the study examines how crosslinking density governs thermal stability and provides a material basis for fracturing of deep reservoirs. Because the demands for proppant transport, clean flowback and fracture-conductivity protection are shared between high-temperature deep reservoirs and heavy-oil intervals, the design principles examined here may also inform low-damage fracturing stimulation of heavy-oil reservoirs, pending dedicated validation [5–7].

2. Results and Discussion

2.1. Construction of the Base Formulation

To engineer a gel system capable of maintaining long-term network integrity under the extreme condition of ≥160 °C, the design of the base formulation must adhere to the principle of structural pre-design. The central strategy is to select a GHPG thickener with outstanding thermal resistance and to ensure that, prior to the formation of a dynamic crosslinked network, the base fluid itself possesses sufficient chain-segment density and

intrinsic viscosity to compensate for the network relaxation induced by intensified molecular thermal motion at elevated temperatures. Through systematic optimization of the GHPG concentration, we established a base formulation endowed with both high thickening efficiency and network-construction potential.

The basic additive package was fixed (0.5 wt% GBA1-2 + 0.5 wt% GBA1-4 + 0.5 wt% GBA1-3 + 0.15 wt% Na_2CO_3 + 0.05 wt% BA-1), while the influence of GHPG concentration (0.50–0.60 wt%) on the apparent viscosity of the base fluid (η_0, FANN-35, 170 s^{-1}, 30 °C) was systematically investigated. This shear rate (170 s^{-1}) corresponds to the typical wall shear condition experienced by fracturing fluids during wellbore flow.

As illustrated in Figure 1, η_0 increased in an approximately linear fashion with rising GHPG concentration. Each data point represents the average of three independent base fluid preparations, with error bars indicating ±1 SD. At a concentration of 0.55 wt%, η_0 reached 87.0 ± 2.1 mPa·s (n = 3), satisfying the minimum threshold of base-fluid viscosity required for proppant transport. Considering that the target reservoir temperature (≥160 °C) far exceeds the tolerance limit of conventional guar gum, the base fluid must provide a sufficient viscosity margin to compensate for the relaxation and partial degradation of the crosslinked network at high temperature. Based on a comprehensive analysis, the optimal GHPG concentration was determined to be 0.55 wt%. At this concentration, the base-fluid viscosity demonstrated the best performance-to-dosage ratio, furnishing a chain-segment density foundation for the crosslinked network studied here.

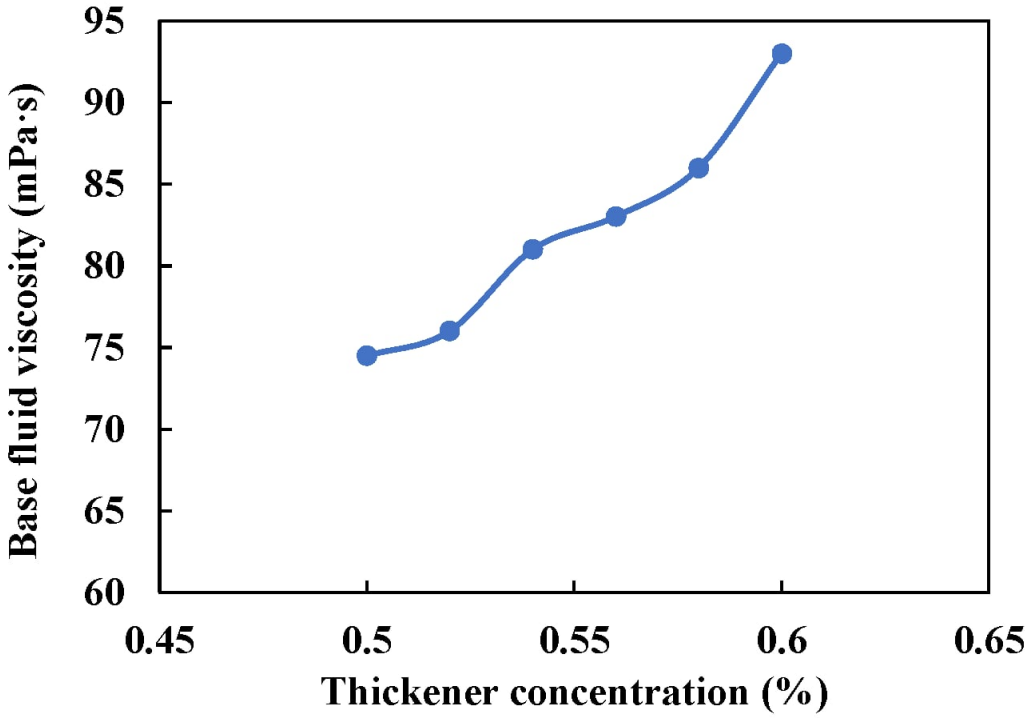


Figure 1. Viscosity variation curves of base fluid under different concentrations of thickener (100 rpm, 170 s^{-1}).

After verifying the compatibility among all components—confirmed by the absence of precipitation or phase separation—the base formulation was established as

0.55 wt% GHPG + 2 wt% KCl + 0.5 wt% GBA1-2 + 0.5 wt% GBA1-4 + 0.5 wt% GBA1-3 + 0.15 wt% Na_2CO_3 + 0.05 wt% BA-1

This formulation serves as the unified material platform for the entire study; all subsequent investigations—crosslinked-network regulation, rheological characterization, and engineering-performance evaluation—were conducted based on it.

2.2. FTIR Band and Rheological Evidence for the Dynamic Covalent Network

Figure 2 compares the relative absorbance at the characteristic FTIR band positions for the base fluid (GHPG only), the sub-threshold gel (0.4 vol% crosslinker), and the optimal gel (0.6 vol% crosslinker); this figure is a peak-position summary comparison, not a continuous recorded spectrum. The GHPG base fluid shows a broad O–H stretching band centered at ~3400 cm^{-1} and a C–O–C stretching band at ~1020 cm^{-1}, characteristic of the polysaccharide backbone. Upon addition of the organoborate crosslinker, a new absorption band appears at ~1340 cm^{-1}, provisionally assigned to the B–O–C stretching vibration of the borate–ester bond; its relative absorbance increases from the sub-threshold to the optimal gel, consistent with a higher density of borate–ester crosslinks. The freeze-dried optimal gel before and after the 160 °C/120 min continuous-shear test likewise retains this band rather than losing it, indicating that the crosslink junctions remain present after high-temperature exposure. These FTIR band observations, together with the frequency-sweep and thixotropic recovery data in Figure 3, provide supportive, rather than stand-alone, evidence for the formation and post-exposure persistence of the borate–ester network. Two qualifications are required. First, FTIR band intensity alone cannot by itself prove bond reversibility; the reversible scission–reformation of the junctions is currently supported by the 140 °C three-step thixotropic recovery test (Sections 2.3 and 4.4), not by a spectroscopic reversibility measurement. Second, in the present study, the raw continuous FTIR traces over 4000–400 cm^{-1} were not retained, and no dedicated post-thermal-treatment spectrum under a controlled aging protocol was acquired; a temperature-cycled FTIR series, combined with temperature-cycling oscillatory rheology and solid-state ^{11}B NMR, would be needed to quantify the reversibility and thermal stability of the B–O–C junctions directly, and these complementary measurements are identified as follow-up work. Accordingly, the high temperature stability observed at 160 °C is attributed to the combined action of the modified rigid backbone, the dense cooperative junction network, and the radical-scavenging stabilizer (Section 2.3), rather than being assigned solely to reversible bond exchange. A further qualification is that the present evidence is spectroscopic (band-level) and rheological; no direct imaging or scattering method (SEM, TEM, cryo-TEM, SAXS or AFM) was applied to resolve the junction-scale network morphology, and the spatial distribution of crosslink density remains inferred rather than observed.

In a dynamic oscillatory test, the storage modulus G′ (Pa) is the elastic (energy-storage) component of the complex shear modulus and quantifies the recoverable, solid-like network response, whereas the loss modulus G″ (Pa) is the viscous (energy-dissipation) component and quantifies the irreversible, liquid-like flow response; the loss factor $\tan\delta = G''/G'$ compares the two. The experimental values reported here are the means of three frequency sweeps at 140 °C and 1.0% strain within the linear viscoelastic region. In addition, the frequency sweep results (Figure 3) provide direct rheological evidence for a critical transition in network topology. For the sub-threshold gel (0.4 vol% crosslinker), both G′ and G″ exhibit a strong frequency dependence, with $G'' > G'$ across the entire frequency range ($\tan\delta > 1$), which is characteristic of a viscous, liquid-like behavior dominated by transient entanglements and a sparse, non-cooperative crosslinked network. In sharp contrast, the optimal gel (0.6 vol% crosslinker) shows $G' > G''$ and G′ is nearly frequency-independent (a plateau modulus), while G″ exhibits a minimum at intermediate frequencies. This frequency response is the hallmark of a system-spanning, elastic gel network, where the relaxation time of the network is longer than the experimental timescale. The plateau in

G′ demonstrates the formation of a stable, self-supporting network. The transition from G″ > G′ to G′ > G″ as the crosslinker concentration increases from 0.4 vol% to 0.6 vol% directly confirms the existence of a critical concentration threshold where the network transforms from a viscous fluid to an elastic gel. We refer to this threshold as the critical crosslinking concentration (c_c = 0.6 vol%), which marks the onset of a cooperative, dynamically self-healing network. A full percolation scaling analysis (e.g., determination of critical exponents) is beyond the scope of the present study but is warranted for future work. On this basis, the percolation-like assignment should be read as an inferential interpretation supported by the frequency-sweep and the band-level FTIR observations: a quantitative percolation analysis (critical exponents, strand-length distribution) and a network model were not fitted to the data, and direct imaging or scattering of the network is left for follow-up work.

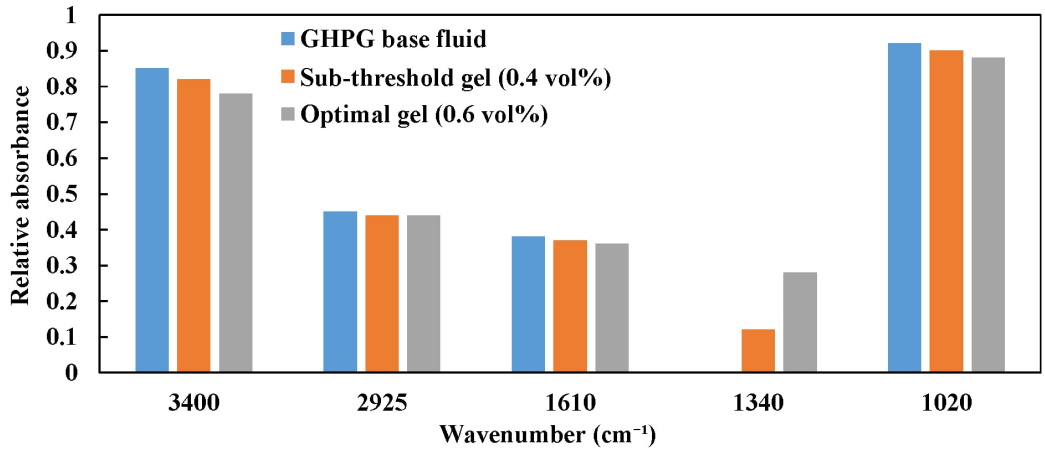


Figure 2. Relative absorbance at the characteristic wavenumbers for the GHPG base fluid, the sub-threshold gel (0.4 vol% crosslinker) and the optimal gel (0.6 vol% crosslinker); band assignments: O–H stretching (~3400 cm^{-1}), aliphatic C–H (~2925 cm^{-1}), H–O–H bending (~1610 cm^{-1}), B–O–C stretching of the borate–ester junction (~1340 cm^{-1}) and polysaccharide C–O–C stretching (~1020 cm^{-1}).

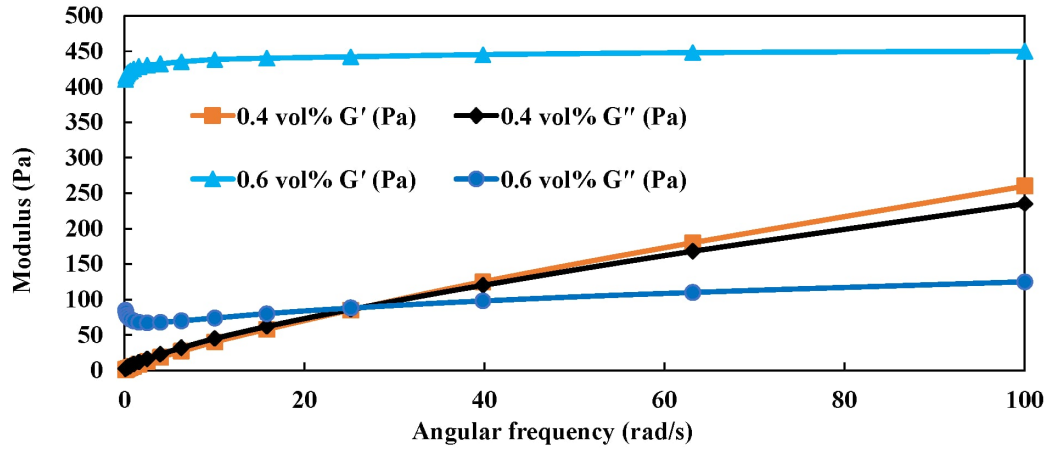


Figure 3. Frequency sweep of storage modulus (G′) and loss modulus (G″) for gels at 140 °C.

2.3. Regulation of Thermal Stability of the Gel Network by Crosslinking Density

The rheological characterization in Section 2.2 has established that the gel with 0.6 vol% crosslinker forms a self-healing elastic network with a distinct yield stress and rapid thixotropic recovery. We now correlate this network architecture with macroscopic thermal stability under continuous shear.

The concentration of the crosslinker is the core parameter governing the crosslinking density of the gel network and thus its structural stability at high temperature. The initial screening of crosslinking density was conducted at 140 °C for two reasons: (i) at this temperature, the borate–ester bond exchange dynamics are sufficiently slow to allow clear differentiation of network behavior across different crosslinker concentrations, yet fast enough to avoid premature thermal degradation of the polymer backbone; and (ii) 140 °C is a standard reference temperature in the literature for characterizing guar-based crosslinked gels [1,10,12], facilitating direct comparison with previously reported systems. By systematically varying the crosslinking ratio (0.1–0.6 vol%) under constant shear at 140 °C and 170 s^{-1}, the structure–property relationship between crosslinking density and network thermal stability was revealed.

The experimental results demonstrate that the temperature and shear resistance of the gel is strongly dependent on the network connectivity, which is determined by the crosslinking-point density and exhibits a distinct threshold behavior. Below a critical crosslinker concentration, the network is sparse and dominated by transient, non-cooperative crosslinks. Under high-temperature shear, the rate of thermal dissociation of borate–ester bonds exceeds the rate of re-formation, leading to irreversible network collapse. When the crosslinking ratio is 0.1–0.3%, the sparse network rapidly disintegrates under the synergistic action of high temperature and shear, with the viscosity plummeting to below 50 mPa·s within 5 min, resulting in a complete loss of proppant-carrying capacity. This indicates that a low-density crosslinked network cannot effectively suppress thermally induced de-crosslinking and segment relaxation. When the crosslinking ratio is increased to 0.4–0.5%, the initial viscosity improves, but the subsequent shearing process is accompanied by pronounced viscosity fluctuations and irreversible decay, signifying that the network is in a dynamic imbalance between crosslinking and de-crosslinking (the "fragile" regime where the system lies near the threshold concentration but has not yet formed a fully cooperative network).

At the threshold of 0.6 vol%, the rheological behavior of the gel undergoes a qualitative transformation. At this concentration, the density of dynamic crosslinks is sufficiently high to create a system-spanning, cooperative network. Under the measurement conditions (140 °C), the frequency sweep data (Figure 3) show $G' > G''$ with a plateau modulus, and the thixotropic recovery test demonstrates rapid recovery of G' after high-shear disruption, indicating that the borate–ester bonds can undergo reversible scission and re-formation on the experimental timescale at this temperature. Macroscopically, this is manifested as the initial viscosity jumping to approximately 1000 mPa·s and, after a brief structural rearrangement, stabilizing rapidly, retaining a viscosity above 190 mPa·s after 120 min of continuous shear.

However, at the target reservoir temperature of 160 °C, the situation is more complex. Borate–ester bonds are inherently labile at elevated temperatures, and irreversible thermal degradation of the glycosidic backbone may also occur. While the thixotropic recovery test at 140 °C provides evidence for dynamic exchange at that temperature, direct confirmation of reversible crosslinking at 160 °C (e.g., through temperature-cycling oscillatory rheology) is beyond the scope of the present study. Therefore, the remarkable thermal stability observed at 160 °C (viscosity > 250 mPa·s for 120 min) is primarily attributed to the synergy of three factors: (i) the rigid hydroxypropyl and carboxymethyl groups introduced into the GHPG backbone, which intrinsically raise the thermal degradation temperature of the individual polymer chains; (ii) the dense dynamic crosslinked network formed at 0.6 vol% crosslinker, which, even if the bond exchange is not fully reversible at 160 °C, provides a high density of crosslinking junctions that slow down network disintegration by increasing the number of bonds that must be broken before chain separation (a "kinetic trapping" effect); and (iii) the

thermal stabilizer GBA1-3 (a thiourea derivative), which acts as a free-radical scavenger and efficiently suppresses thermo-oxidative chain scission. The possible contribution of dynamic bond exchange (scission-recombination) to stress dissipation at 160 °C remains a hypothesis that requires further experimental validation, but the combined effects of the rigid backbone, high crosslink density, and radical trapping are sufficient to explain the observed performance.

Accordingly, the optimal crosslinking ratio was determined to be 0.6 vol%. This finding identifies a crosslinker-concentration threshold—the cc = 0.6 vol% value introduced above—for engineering gels with tailored stability for high-temperature applications, while acknowledging that the underlying mechanism combines kinetic stabilization with, possibly, dynamic bond exchange.

2.4. Evaluation of Long-Term Thermal Stability of the Gel

2.4.1. Long-Term Stability at 160 °C

Based on the optimal crosslinking ratio (0.6 vol%), long-term shear tests were first conducted under the standard condition of 160 °C and 170 s^{-1} using the pressurized sealed cell (2 MPa N_2), and the results are presented in Figure 4. The gel exhibited outstanding long-term thermal stability: after an initial structural rearrangement (~5 min), the apparent viscosity remained stable at approximately 350 mPa·s for 60 min, and after 120 min of continuous shear, the viscosity was still maintained above 250 mPa·s, with the viscosity–time curve leveling off. This plateau behavior directly contradicts the hypothesis of evaporation-induced level drop; if evaporation were significant, a continuous, accelerating decline would be observed. Figure 4 presents the mean viscosity values from three independent experiments, with shaded regions representing ±1 SD. The standard deviation increased from ±5 mPa·s at 60 min to ±12 mPa·s at 120 min, indicating slightly higher variability at longer shearing times but remaining within acceptable limits (±5% of the mean). This performance is realized through the synergistic contribution of three aspects: (i) the rigid groups introduced into the GHPG molecular backbone intrinsically raise the thermal degradation temperature of the individual macromolecular chains; (ii) the dense dynamic crosslinked network formed at 0.6 vol% crosslinking ratio effectively distributes local stresses and can dissipate energy and repair defects through the dynamic scission–recombination process; and (iii) the thermal stabilizer (GBA1-3), acting as a free-radical scavenger, efficiently suppresses the thermo-oxidative chain degradation triggered by dissolved oxygen or persulfate residues. The reported stability is bounded by the 120 min continuous-shear window of this test; chemical stability and viscosity retention beyond 120 min at 160 °C were not explored, and longer aging is required before extrapolating to extended treatment times.

2.4.2. Extended Validation at 180 °C (Without Breaker)

To directly validate the thermal stability of the gel at the upper end of the target temperature range (180 °C) in the absence of chemical breaker, an additional long-term isothermal shear test was performed at 180 °C and 170 s^{-1} using the same gel formulation (0.6 vol% crosslinker) without adding ammonium persulfate. The results are shown in Figure 5. The gel maintained an apparent viscosity above 120 mPa·s after 60 min of continuous shear and above 80 mPa·s after 90 min. Although the viscosity at 180 °C is lower than that at 160 °C due to accelerated thermal motion and bond exchange dynamics, the gel still exhibits acceptable proppant-carrying capacity (viscosity > 50 mPa·s) for the first 70 min. After 100 min, the viscosity gradually declines to below 50 mPa·s, indicating the onset of network degradation. These results confirm that the GHPG dynamic covalent gel can maintain functional integrity for approximately 60–90 min at 180 °C without chemical breaker, which is sufficient for typical fracturing treatment durations in ultra-deep reservoirs. The reduced

stability at 180 °C compared with 160 °C is consistent with the temperature-accelerated dissociation of borate–ester bonds, but the system remains viable for the required operational window. As at 160 °C, the 180 °C observation is limited to the 90 min test window; behavior beyond 90 min without breaker was not characterized. In Figure 5, the left ordinate is the apparent viscosity (mPa·s, range 200–2200) and the right ordinate is the shear rate (s^{-1}, range 150–180); the abscissa is the shearing time (min, 0–150), and the blue viscosity trace is read against the left axis. On this scale, the viscosity initially rises to about 1800 mPa·s during the structural rearrangement, then decays toward the measured plateau: it remains above 120 mPa·s after 60 min and above 80 mPa·s after 90 min, stays above 50 mPa·s for the first 70 min, and falls below 50 mPa·s only after 100 min.

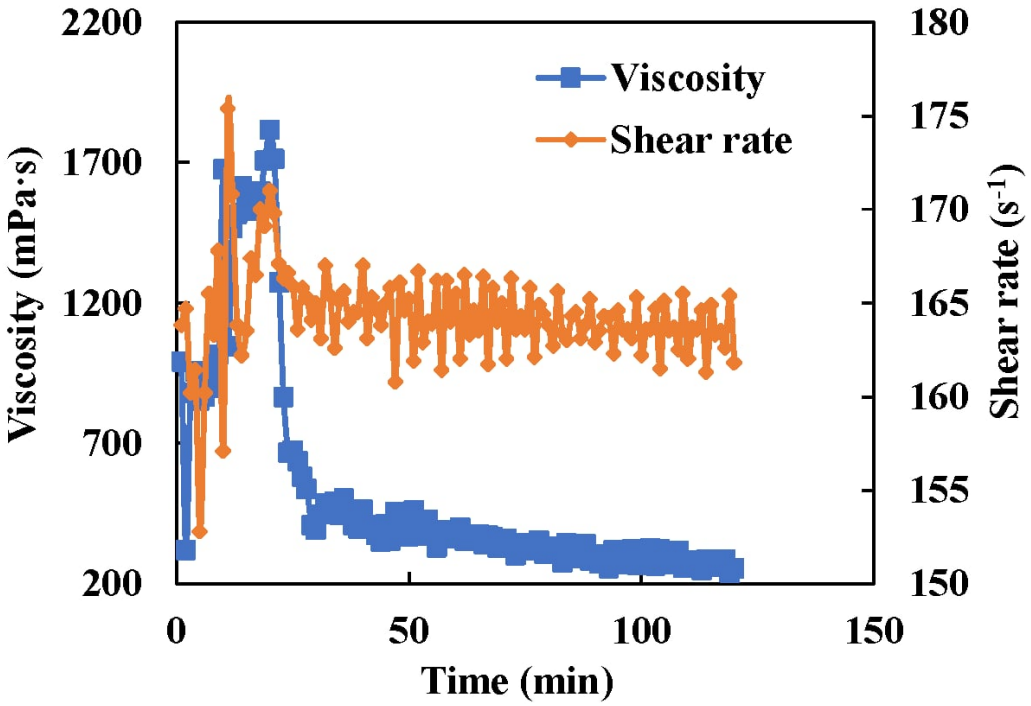


Figure 4. Viscosity–time curve of the fracturing fluid at 160 °C.

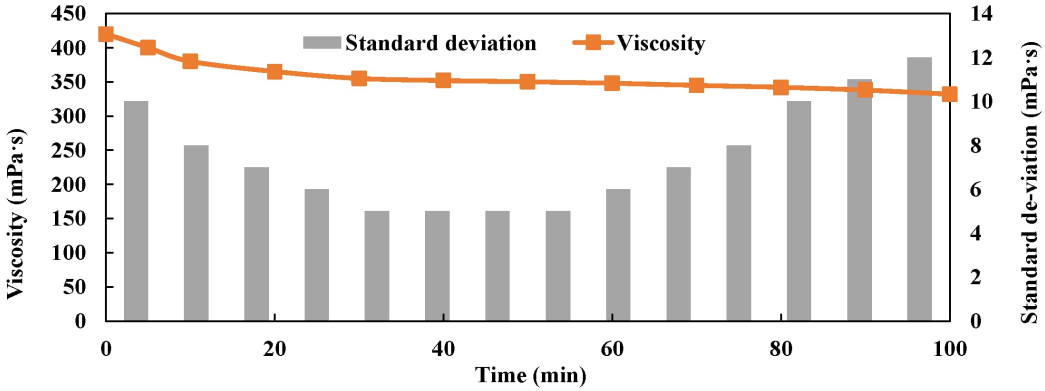


Figure 5. Viscosity–time curve at 180 °C and 170 s^{-1} without breaker (n = 3, mean ± SD), demonstrating the intrinsic thermal stability of the gel at the upper temperature limit.

2.4.3. Control Experiment with Commercial Hydroxypropyl Guar (HPG)

To directly quantify the performance advantage of our GHPG-based dynamic covalent gel over a conventional system, a control experiment was conducted using a commercial hydroxypropyl guar (HPG, Mw ≈ 2.0 × 10^6 Da, DS ≈ 0.35) crosslinked with a standard

organoboron crosslinker (borax, 0.5 wt% in the base fluid). The HPG-borate system was selected as the commercial benchmark because it represents the most widely used industrial formulation for high-temperature fracturing operations [1,10,21]. This comparison is intended to evaluate the overall engineering performance of our system against an established industrial standard, rather than to isolate the effect of the thickener alone (which is addressed by the crosslinker-free GHPG control in Section 2.4.4). The base fluid composition was otherwise identical to that used for GHPG (0.55 wt% polymer, 2 wt% KCl, pH = 10.8). The long-term isothermal shear test was performed at 160 °C and 170 s^{-1} using the same pressurized sealed cell (2 MPa N_2) to ensure comparability. As shown in Figure 6, the conventional HPG-borate gel exhibited a rapid viscosity decline, dropping to below 100 mPa·s within 60 min and to approximately 45 mPa·s after 120 min. This behavior is consistent with the well-known thermal instability of borate-crosslinked guar at elevated temperatures, primarily due to the irreversible thermo-oxidative scission of the glycosidic backbone and the lability of borate–ester bonds above 140 °C. In contrast, our GHPG-based gel (0.6 vol% organoborate crosslinker) maintained a viscosity above 250 mPa·s after 120 min under identical conditions. This direct comparison quantitatively demonstrates that the percolation-controlled dynamic network in GHPG, combined with its rigid modifying groups and thermal stabilizer, provides significantly enhanced thermal stability relative to a commercial benchmark. This control represents one commercial HPG–borate benchmark; no second commercial formulation or manufacturer-grade product was included in the comparison, so the contrast is representative rather than exhaustive across field-grade fluids.

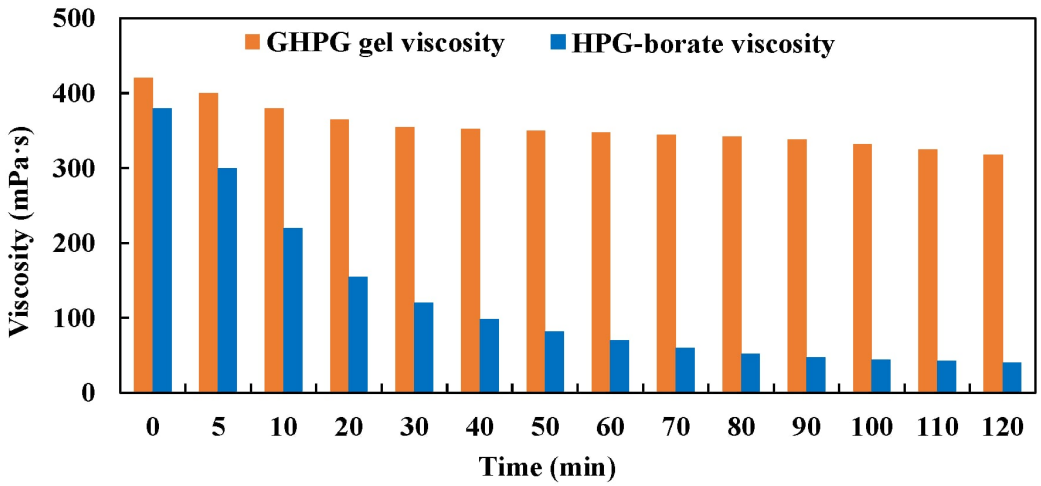


Figure 6. Viscosity-time curves at 160 °C and 170 s^{-1} comparing the optimal GHPG gel (0.6 vol% crosslinker) with a commercial HPG-borate control (0.5 wt% borax). All conditions are identical.

2.4.4. Control Experiment: GHPG Base Fluid Without Crosslinker

To unambiguously demonstrate the contribution of the borate–ester crosslinked network to the high-temperature stability, a control experiment was performed using the same GHPG base fluid (0.55 wt% GHPG, 2 wt% KCl, pH = 10.8, and all functional additives except the crosslinker GBA1-1) under identical conditions: 160 °C, 170 s^{-1}, pressurized sealed cell (2 MPa N_2). As shown in Figure 7, the crosslinker-free GHPG base fluid exhibited a rapid and continuous viscosity decline, dropping from an initial value of approximately 210 mPa·s to below 50 mPa·s within 20 min and to approximately 25 mPa·s after 120 min. This behaviour is consistent with the thermo-oxidative degradation of the guar backbone in the absence of a protective crosslinked network. In stark contrast, the optimally crosslinked GHPG gel (0.6 vol% GBA1-1) maintained a viscosity above 250 mPa·s throughout the

120 min test under identical conditions. This direct comparison quantitatively demonstrates that the remarkable thermal stability of our system is not merely an intrinsic property of the modified GHPG polymer, but is critically dependent on the formation of a dense, dynamic borate–ester crosslinked network that provides structural integrity and resistance to thermal degradation. The crosslinked network effectively suppresses chain segmental mobility, slows thermo-oxidative scission, and enables dynamic bond exchange for network self-repair.

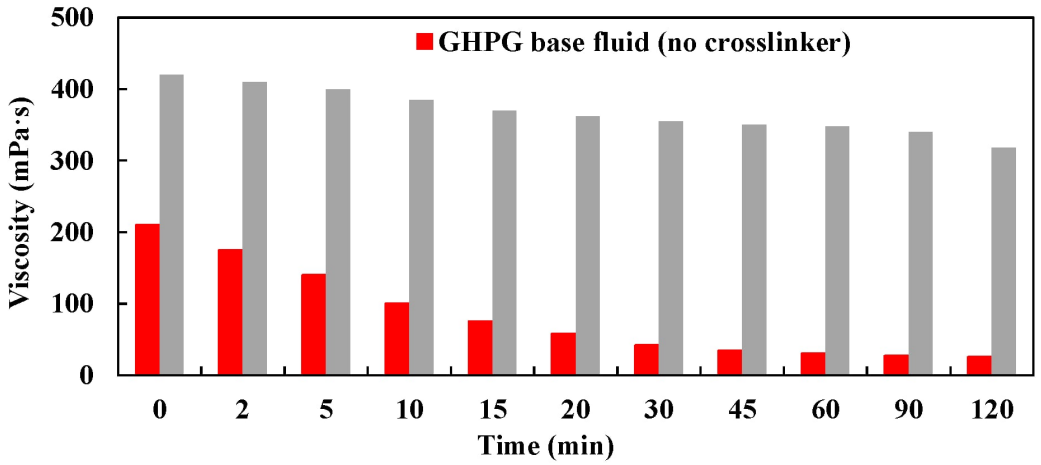


Figure 7. Comparison of viscosity-time curves at 160 °C and 170 s^{-1} between the GHPG base fluid without crosslinker and the optimally crosslinked GHPG gel (0.6 vol% GBA1-1). Data points represent mean ± SD (n = 3).

2.5. High-Temperature Triggered Controllable Gel Breaking

At 180 °C, after the intrinsic thermal stability of the gel was characterized (Section 2.4.2), 50 ppm of ammonium persulfate (APS) breaker was injected into a fresh gel sample at the same temperature, and the viscosity decay curve was recorded under continuous shear at 170 s^{-1}. The gel-breaking kinetics exhibited a typical rapid-response characteristic. The extremely short half-life of APS at 180 °C (ca. 5–8 min) leads to its rapid thermal decomposition, generating a high concentration of sulfate radicals ($SO_4^{-}\cdot$). These highly reactive radicals simultaneously attack the glycosidic bonds on the GHPG backbone and the borate–ester crosslinking junctions within the network, causing the three-dimensional network to undergo synergistic disintegration at the molecular level. Macroscopically, this process is manifested as a sharp drop in viscosity: the system viscosity decreases to approximately 50 mPa·s within 30 min and falls below 10 mPa·s within 70 min, achieving deep and complete gel breaking.

Together, Sections 2.4.2 and 2.5 demonstrate that at 180 °C, the gel maintains sufficient stability for field operations (viscosity > 80 mPa·s for > 90 min) in the absence of a breaker, yet undergoes rapid and thorough disintegration upon breaker injection. This dual capability confirms the applicability of the GHPG-based dynamic crosslinked network for fracturing operations in ultra-deep reservoirs with bottom-hole temperatures up to 180 °C.

2.6. Engineering Applicability

The preceding sections have demonstrated that the constructed GHPG dynamic crosslinked network simultaneously possesses outstanding long-term thermal stability and on-demand rapid gel-breaking capability over the temperature range of 160–180 °C. The ultimate engineering value of a fracturing fluid, however, is determined by its integrated performance under simulated field conditions. This section systematically evaluates the

potential of the gel system for practical application from the perspectives of friction control, fluid-loss and formation protection, and compatibility with formation fluids.

2.6.1. Friction Characteristics and Drag Reduction Performance

The friction pressure drop generated by turbulent flow of the fracturing fluid in the tubing directly governs the wellhead pumping pressure and constitutes a critical engineering parameter affecting operational safety and energy consumption. The drag reduction performance of the gel system under various pipe diameters, flow rates, and temperature conditions was evaluated using a multi-functional flow-loop system (Loop sys, equipped with dual-pipe loops of 62 mm and 76 mm diameters and high-precision differential pressure transducers). The drag reduction rate (DR%) was calculated with the friction pressure drop of fresh water under identical conditions as the baseline. The characteristic parameters for pipe flow of power-law fluids—flow behavior index (n) and consistency coefficient (K)—were obtained by double-logarithmic regression of the shear stress versus shear rate relationship, and the friction pressure gradient along the pipe was calculated according to Equations (1)–(5): Equations (1)–(5) are the standard pipe-flow relations for a power-law (Ostwald–de Waele) fluid; they are not derived in this study but are adopted from conventional rheology and hydraulic-fracturing flow-loss/pipe-flow practice, and are used here only to reduce the measured torque–shear-rate and pressure-drop data. Equation (1) gives the apparent wall shear rate $\dot{\gamma} = 4Q/(\pi R^3)$ from the volumetric flow rate and pipe radius; Equation (2) gives the wall shear stress $\tau = \Delta P \cdot R/(2L)$ from the measured pressure drop over the pipe length; Equations (3) and (4) fit the two parameters of the power-law constitutive relation $\tau = K \cdot \dot{\gamma}^n$, where n is the dimensionless flow behavior index ($n < 1$ for a shear-thinning gel) and K is the consistency coefficient; Equation (5) then estimates the frictional pressure gradient $\Delta P/L$ along the pipe for that power-law fluid. The physical meaning of each term is stated in the Nomenclature sentence below.

Shear rate:

$$\gamma = \frac{4Q}{\pi R^3} \tag{1}$$

Shear stress:

$$\tau = \frac{\Delta P \cdot R}{2L} \tag{2}$$

The flow behavior index and consistency coefficient are determined by double-logarithmic regression:

$$n = \frac{d(\log \tau)}{d(\log \gamma)} \tag{3}$$

$$K = \frac{\tau}{\gamma^n} \tag{4}$$

Frictional pressure gradient along the pipe:

$$\frac{\Delta P}{L} = \frac{2K}{D}\left(\frac{8Q}{\pi R^3}\right)^n \tag{5}$$

where Q is the flow rate (m^3/min), R is the internal pipe radius (m; D = 2R), D is the pipe diameter (m), ΔP is the pressure drop (Pa), L is the pipe length (m), $\dot{\gamma}$ is the wall shear rate (s^{-1}), τ is the wall shear stress (Pa), n is the flow behavior index, and K is the consistency coefficient ($Pa \cdot s^n$).

The test results are summarized in Table 1 and Figure 8. The data reveal that the drag reduction rate increases monotonically with increasing flow rate, and the effect is more pronounced in the smaller 62 mm pipe. At 40 °C and 6.0 m^3/min, the drag reduction rate reaches 58.02%; at 80 °C and the same flow rate, it remains 53.73%. The drag reduction rate (DR%) was calculated against fresh water measured in the same loop, same pipe diameter,

same flow rate, and same temperature, using $DR\% = (\Delta P_{water} - \Delta P_{gel})/\Delta P_{water} \times 100\%$, where ΔP is the measured friction pressure drop over the calibrated pipe section. This fresh water reference isolates the friction contribution of the polymer network from pipe geometry and flow-rate effects. The 58.02% value means that, under the 62 mm/6.0 m^3/min/40 °C conditions, the gel produces about 42% lower turbulent friction pressure drop than water, reducing wellhead pumping load and energy consumption while preserving the viscosity required for proppant transport. The relatively mild temperature effect indicates that the viscoelastic characteristics of the system have not deteriorated substantially over the 40–80 °C range sampled in the loop. This favorable drag reduction originates from molecular-chain extension and elastic energy storage of the macromolecular segments under turbulent vortex stretching, which suppress momentum transfer among turbulent eddies and thereby reduce wall friction.

Table 1. Drag reduction rates of the fracturing fluid system under various conditions.

Temperature/°C	Pipe Diameter/mm	Drag Reduction Rate Under Different Flow Rates/%							
		1.0 m^3/min	2.0 m^3/min	3.0 m^3/min	4.0 m^3/min	5.0 m^3/min	6.0 m^3/min	7.0 m^3/min	8.0 m^3/min
40	62	5.99 ± 0.36	11.41 ± 0.68	28.54 ± 1.71	40.46 ± 1.21	48.82 ± 1.46	58.02 ± 1.74	64.35 ± 1.93	69.78 ± 2.09
40	76	6.92 ± 0.42	9.99 ± 0.60	18.29 ± 1.10	26.31 ± 0.79	36.08 ± 1.08	46.06 ± 1.38	51.28 ± 1.54	55.63 ± 1.67
80	62	5.03 ± 0.30	11.85 ± 0.71	27.94 ± 1.68	39.92 ± 1.20	47.98 ± 1.44	53.73 ± 1.61	59.16 ± 1.77	63.85 ± 1.92
80	76	7.51 ± 0.45	10.19 ± 0.61	16.61 ± 1.00	26.72 ± 0.80	37.99 ± 1.14	46.99 ± 1.41	52.74 ± 1.58	57.29 ± 1.72

Note: All drag reduction rates are reported as mean ± SD from three independent flow-loop experiments (n = 3). The relative standard deviation (RSD) was consistently below 3% for flow rates ≥ 4.0 m^3/min and below 6% for lower flow rates.

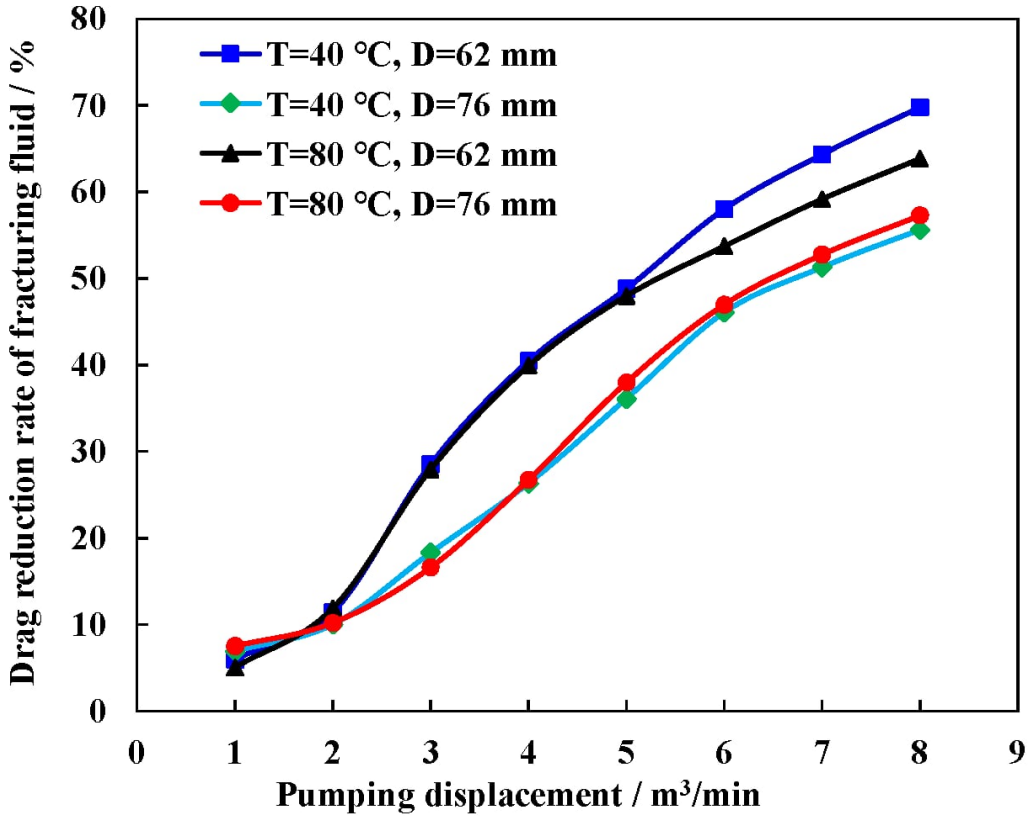


Figure 8. Drag reduction rate curves of GHPG under different pipe diameters and temperatures.

2.6.2. Engineering Quality of the Broken-Gel Fluid

After the fracturing operation, the characteristics of low viscosity, low surface tension, and low solid residue content of the broken-gel fluid are critical engineering quality indica-

tors that ensure efficient flowback and minimize secondary formation damage. Based on the 180 °C/50 ppm APS gel-breaking conditions established in Section 2.5, surface tension and residue content analyses were conducted on the supernatant of the thoroughly broken gel fluid (viscosity < 10 mPa·s).

The surface tension of the supernatant was measured by the pendant-drop method at ambient temperature, yielding values of 27.3 mN/m and 27.1 mN/m for two parallel tests (Table 2). This value is substantially lower than the surface tension of fresh water (ca. 72 mN/m), confirming that the cleanup additive GBA1-13 retains excellent interfacial activity after exposure to 180 °C. It can effectively reduce the capillary resistance of the broken fluid in formation pores and significantly enhance the flowback efficiency.

Table 2. Surface tension test results of the broken-gel fluid (n = 3 independent gel-breaking experiments, with two parallel measurements per experiment).

Sample	Broken-Gel Viscosity/mPa·s	Surface Tension/mN·m^{-1}
1	3	27.3
2	3	27.1
3	3	27.2
Mean ± SD	3.0 ± 0.0	27.2 ± 0.1

The solid residue content is an important indicator for evaluating the potential plugging risk of fracturing fluids to formation pore throats and fracture conductivity. A 500 mL aliquot of the above broken-gel fluid (initial GHPG concentration 0.55 wt%) was centrifuged at 3000 r/min for 30 min to separate the insoluble matter, and the precipitate was dried at 105 °C to constant weight for quantification. The measured residue content was 534 mg/L, which is below the maximum residue limit of 600 mg/L stipulated by the industry standard SY/T 6376-2008 [29]. This result (Table 3) demonstrates that although GHPG carries rigid modifying groups incorporated to meet the stability requirement above 160 °C, it can still degrade into water-soluble low-molecular-weight fragments after high-temperature oxidative gel breaking, with the solid residue remaining within a controllable range and satisfying the engineering requirement of low residue for high-temperature reservoir fracturing.

Table 3. Solid residue test results (n = 3 independent gel-breaking and centrifugation experiments).

Parameter	Value (Mean ± SD)
Sampling volume/mL	60 (fixed)
Empty tube mass/g	25.0 (tare)
Total mass after drying/g	25.032 ± 0.008
Residue content/mg·L^{-1}	534 ± 21
Residue ratio/%	0.13 ± 0.01

2.6.3. Dynamic Fluid Loss and Wall-Building Performance

The fluid-loss characteristics of a fracturing fluid directly influence the liquid efficiency and the dimensions of the created fractures. Dynamic fluid-loss experiments were performed using a high-temperature, high-pressure dynamic fluid-loss apparatus. The initial screening experiments were conducted at 90 °C and 10 MPa differential pressure, which is a standard condition recommended by the Chinese oil and gas industry standard SY/T 5107-2016 for comparative evaluation of fracturing fluid-loss performance [30]. This temperature was selected for the following reasons: (i) it allows direct comparison with published data on conventional guar-based fracturing fluids, most of which were tested under similar moderate-temperature conditions; (ii) it provides a baseline for understanding the fluid-loss behavior of the crosslinked network before extrapolation to higher temperatures;

and (iii) at the time of this study, the available dynamic filtration apparatus was certified for safe operation only up to 120 °C.

To directly assess fluid-loss performance under conditions representative of the target ultra-deep reservoir (160–180 °C), additional dynamic fluid-loss experiments were subsequently performed at 160 °C using an upgraded high-pressure, high-temperature filtration system (maximum operating temperature 200 °C). The core sample used for the 160 °C test was selected from the same reservoir block (Well T2, 6953.7 m, permeability 5.05 mD, porosity 8.1%). The differential pressure was maintained at 10 MPa, and the shear rate was 170 s^{-1}, consistent with the low-temperature tests. Thus, the 90 °C data serve as a benchmark for literature comparison, while the 160 °C data validate the performance under realistic ultra-deep reservoir conditions.

The filtrate volume was recorded against the square root of filtration time; the slope m and intercept h of the resulting linear segment were obtained by linear regression of the measured filtrate-volume data (the curve itself is not reproduced as a figure in this manuscript). The filter-cake-controlled fluid-loss coefficient C_3, the filtration velocity vc, and the spurt-loss volume Qsp are calculated according to Equations (6)–(8):

$$C_3 = \frac{m}{2A} \tag{6}$$

$$v_c = \frac{C_3}{\sqrt{t}} \tag{7}$$

$$Q_{sp} = \frac{h}{A} \tag{8}$$

where m is the slope of the filtration curve (mL/$min^{0.5}$); A is the filtration area (cm^2); C_3 is the filter-cake-controlled fluid-loss coefficient (m/$min^{0.5}$); v_c is the filtration velocity (m/min); h is the intercept of the filtration curve on the Y-axis (cm^3); Q_{sp} is the spurt-loss volume (m^3/m^2); and t is the filtration time (min).

Core parameters: Diameter: 2.54 cm; length: 3.36 cm; filtration area: 4.95 cm^2; permeability: 12.38 mD (Table 4). The experiments were conducted at 90 °C under a differential pressure of 10 MPa, with a shear rate of 170 s^{-1} and a dynamic filtration duration of 2 h.

Table 4. Dynamic fluid-loss coefficient measurement results (90 °C, baseline screening).

Parameter	Value (Mean ± SD, n = 3)
Core diameter/cm	2.54 (fixed)
Core length/cm	3.36 (fixed)
Filtration area/cm^2	4.95 (fixed)
Permeability/mD	12.38 ± 0.52
Fluid density/g·cm^{-3}	1.000 (reference)
Dynamic fluid-loss coefficient/m·$min^{-0.5}$	(3.76 ± 0.14) × 10^{-4}

The realization of this low fluid-loss coefficient at elevated temperatures is attributed to the rapid formation of a dense dynamic filter cake by the GHPG gel on the core end-face under differential pressure. As confirmed in Sections 2.2 and 2.3, the three-dimensional critical crosslinking network constructed at 0.6 vol% possesses dense and self-healable structural characteristics. Even at 160 °C (Table 5), where the borate–ester bond exchange dynamics are accelerated, the network retains sufficient integrity to form an effective filter cake, as evidenced by the C_3 value of 6.89 × 10^{-4} m/$min^{0.5}$. When the gel contacts the core end-face, the high-density dynamic covalent crosslinked network can rapidly dehydrate and concentrate under differential pressure and shear to form a low-permeability polymeric filter-cake barrier, effectively retarding continuous fluid loss into the deep formation.

Table 5. Dynamic fluid-loss coefficient at representative high temperature (160 °C).

Parameter	Value
Core plug source	Well T2 (6953.7 m)
Permeability/mD	5.05
Porosity/%	8.1
Temperature/°C	160
Differential pressure/MPa	10
Shear rate/s^{-1}	170
Filtration duration/min	60
Dynamic fluid-loss coefficient C_3/m·$min^{-0.5}$	6.89×10^{-4} (n = 2, range: 6.71–7.07 × 10^{-4})
Spurt-loss volume Q_{sp}/m^3·m^{-2}	8.2×10^{-6}

Note: The high-temperature fluid-loss tests were limited by the availability of the upgraded HPHT filtration system and the restricted number of preserved core plugs from the ultra-deep reservoir. The two independent measurements showed good consistency (variation < 5.5%). Because the replicate count is small, these results should be regarded as preliminary evidence of fluid-loss control under representative conditions rather than a statistically representative characterization; a larger set of core plugs is needed to bound the spread in C_3.

2.6.4. Formation Damage Performance and Mechanism Analysis

The formation damage evaluation (Sections Core-Matrix Damage and Fracture-Conductivity Damage) was conducted under simulated reservoir conditions (90 °C for core-matrix damage, 25–85 MPa closure stress for fracture conductivity). While the core-matrix damage temperature (90 °C) is lower than the target reservoir temperature (160–180 °C), this temperature was chosen to be consistent with the industry standard (SY/T 6376-2008) for comparative evaluation. The damage mechanisms (residue plugging, filtrate invasion, polymer layer formation) are expected to be qualitatively similar at higher temperatures, though the absolute damage rates may differ. We note that a direct damage evaluation at 160 °C was not performed due to equipment limitations, and this represents a limitation of the current study. The fracture conductivity damage tests were performed at ambient temperature after gel breaking at 180 °C, which is representative of the post-treatment condition in the fracture.

Due to the limited availability of preserved reservoir core plugs from ultra-deep wells, the damage evaluation was performed on three representative samples. While this sample size is modest, the three cores cover a range of permeabilities and mineral compositions typical of the target formation, and the damage rates obtained are highly consistent (SD = 1.2%). Therefore, the results provide a reliable indication of the gel system's formation-protection performance, although a larger-scale statistical study would be beneficial for future field-specific optimization. In addition, the matrix-damage and conductivity evaluations were each performed on a small number of parallel samples (three core plugs; three conductivity replicates); variability across broader core populations and clay types was therefore not sampled.

Core-Matrix Damage

Three reservoir core plugs from the peripheral TH Oilfield were selected, and dynamic displacement experiments in both forward and reverse directions were performed under simulated formation conditions (90 °C, 10 MPa differential pressure, shear rate 170 s^{-1}) to measure the permeability change before and after contamination by the broken-gel fluid. As listed in Table 6, the matrix permeability damage rates for the three cores were 18.5%, 16.7%, and 16.2%, with an average value below 18%. This damage level is lower than the typical range reported for conventional guar-gum fracturing fluid systems (>25%), with the caveat that literature values derive from different core and test conditions.

Table 6. Core-matrix damage test results of the fracturing fluid.

Core No.	Well ID (Depth)	Porosity/%	Major Minerals (XRD)	Wettability (Contact Angle)	Initial Permeability/ 10^{-3} μm²	Post-Contamination Permeability/ 10^{-3} μm²	Damage Rate/%	Test Conditions
1	T1 (6902.0 m)	6.8	Quartz 72%, Feldspar 18%, Clays 7%	Water-wet, θ = 52°	3.30	2.69	18.5	ΔP = 10 MPa, τ = 170 s^{-1}, T = 90 °C, t = 2 h
2	B2 (6031.7 m)	5.2	Quartz 75%, Feldspar 15%, Clays 6%	Water-wet, θ = 48°	1.61	1.34	16.7	Same as above
3	T2 (6953.7 m)	8.1	Quartz 68%, Feldspar 20%, Clays 8%	Intermediate, θ = 58°	5.05	4.23	16.2	Same as above
Mean ± SD		–	6.7 ± 1.5	–	–	3.32 ± 1.73	2.75 ± 1.45	17.1 ± 1.2

Note: The high SD in permeability and porosity reflects natural core heterogeneity, typical for reservoir core plugs. The damage rate, however, shows much lower variability (RSD ≈ 7%), indicating consistent formation protection performance across different core types. Wettability was measured by the sessile drop method on cleaned core surfaces using formation water. Clay content was quantified by XRD, with illite and kaolinite as the dominant clay species.

The relatively low matrix damage rate is consistent with the thorough gel breaking, the low measured residue, and the dense dynamic filter cake reported above; the specific damage mechanisms are analyzed in the following paragraph against the measured data.

The observed matrix permeability damage (16.2–18.5%) can be attributed to three main mechanisms based on the combined experimental evidence. First, the measured residue content (534 ± 21 mg/L, Table 3) indicates that a small amount of water-insoluble polymer fragments remains after gel breaking. These fragments can physically block pore throats, especially in lower-permeability cores (e.g., Core 2 with 1.61 mD). Second, the dynamic fluid-loss coefficient (3.76×10^{-4} m/$min^{0.5}$, Table 4) suggests that some filtrate invades the matrix during the experiment; this filtrate contains residual oligosaccharides and additives that may adsorb onto clay surfaces or alter the local water saturation, causing water-block or minor clay swelling. The relatively low clay content (<8 wt%) and the water-wet nature of the cores, however, minimize the contribution of clay swelling. Third, the dynamic crosslinked network itself, while effective in forming a low-permeability filter cake, may leave a thin polymer layer on the core end-face that is not completely removed by back-flow. Transmission electron microscopy (TEM) or scanning electron microscopy (SEM) of the damaged core surfaces would be required to directly visualize these residual deposits, which is planned for a follow-up study. Despite these multiple damage contributors, the overall damage rate remains below 19%, which is substantially lower than that of conventional guar-based fluids (>25%), confirming the low-damage characteristic of the designed gel system. At the network level, the present study did not apply SEM, TEM, cryo-TEM, SAXS or AFM to image the crosslinked gel itself; the residue and deposit descriptions above rest on rheology, band-level FTIR observations and core-permeability evidence. Direct morphology imaging is planned as a follow-up.

Fracture-Conductivity Damage

An API standard conductivity cell was employed to simulate a propped fracture at a sand concentration of 10 kg/m^2, and the damage of the broken-gel fluid to fracture conductivity was evaluated. As presented in Table 7, over the range of increasing closure stress from 25.0 MPa to 85.0 MPa, the damage rate progressively rises from 7.27% to 14.64%. Even under

the high closure stress of 85.0 MPa, the damage rate is merely 14.64%, significantly lower than that of conventional organometallic crosslinked fracturing fluids (typically > 25%).

Table 7. Fracture-conductivity damage test results by the broken-gel fluid.

Closure Stress/MPa	Conductivity Before Damage/μm²·cm	Conductivity After Damage/μm²·cm	Damage Rate/%
25.0	154.3 ± 8.0	143.0 ± 7.0	7.27
35.0	145.4 ± 7.0	133.4 ± 7.0	8.23
45.0	138.8 ± 7.0	126.0 ± 6.0	9.22
55.0	116.5 ± 6.0	103.2 ± 5.0	11.45
65.0	105.3 ± 5.0	90.8 ± 5.0	13.79
75.0	84.6 ± 4.0	71.2 ± 4.0	15.74
85.0	75.9 ± 4.0	64.8 ± 3.0	14.64

Note: Each conductivity value represents the mean of three independent fracture conductivity experiments (n = 3) using freshly prepared proppant packs and gel samples. The standard deviation for conductivity measurements was typically within ±5% of the mean.

The increasing trend of damage rate with rising closure stress can be ascribed to the intensified embedment of proppant particles into the fracture walls under high closure stress (Figure 9), which geometrically amplifies the plugging effect of minute polymer residues remaining on the fracture surfaces on the conductive pathways. Owing to the thorough gel breaking (final viscosity < 10 mPa·s) and low residue ratio of this system, however, the residual fluid within the fracture can be effectively removed after flowback. Consequently, more than 85% of the conductivity is retained even at the highest closure stress tested, indicating that the gel limits conductivity impairment under these conditions.

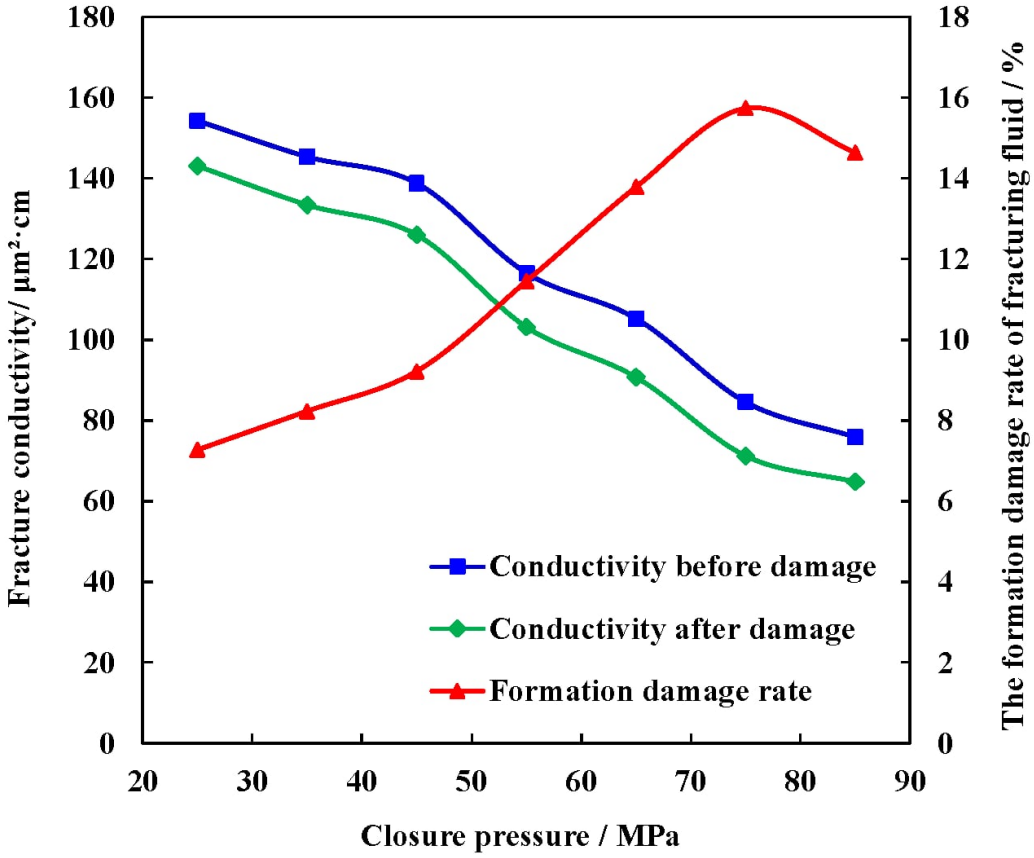


Figure 9. Comparison of fracture conductivity before and after damage.

2.6.5. Compatibility with Formation Water

The formation water in ultra-deep reservoirs is typically characterized by high salinity and high hardness (rich in ions such as Ca^{2+} and Mg^{2+}). When an extraneous fluid enters the reservoir, if the residual polymer fragments or functional additives in the broken-gel fluid form insoluble complexes or inorganic precipitates with the polyvalent metal ions in the formation water, severe chemical-scale plugging will occur, and the resulting damage may often exceed the physical plugging caused by solid residues. Compatibility evaluation therefore serves as the last critical barrier for assessing the engineering applicability of the gel system.

Actual formation water from the peripheral TH Oilfield was mixed with the gel fluid that had been thoroughly broken at 180 °C (viscosity < 10 mPa·s) at volumetric ratios of 2:1, 1:1, and 1:2, and the mixtures were observed after standing at the reservoir temperature of 70 °C for 2 h. At all mixing ratios, only minute amounts of flocculent matter appeared, with the total precipitated amount below 0.1%; no distinct inorganic scaling or emulsified phase separation was observed.

This favorable compatibility is rooted in chemical compatibility in two respects: first, Section 2.5 has demonstrated that under APS triggering the gel undergoes deep scission of both glycosidic bonds and borate–ester crosslinking bonds, yielding predominantly water-soluble oligosaccharide fragments as the degradation products, with a limited number of residual chelating groups on the molecular chains that are unlikely to form crosslinked precipitates with Ca^{2+} and Mg^{2+}; second, the functional additives (GBA1-13, GBA1-5, etc.) selected in the formulation were screened during the formulation-design stage for their chemical structural types compatible with high-salinity brines. These results indicate that the ultra-high-temperature gel system possesses excellent chemical compatibility with the reservoir fluids of the peripheral TH Oilfield, can avoid secondary formation damage caused by fluid incompatibility, and provides an important safety guarantee for its field application.

2.6.6. Comparison with Literature Data

To benchmark the performance of our GHPG dynamic covalent gel against existing ultra-high-temperature fracturing fluids, Table 8 summarizes key parameters from representative studies published in the last five years. The selected references include both guar-derived systems (e.g., organoboron-crosslinked hydroxypropyl guar) and synthetic polymer gels (e.g., polyacrylamide-zirconium, supramolecular reinforced gels). All values are taken directly from the cited sources or calculated from their reported data where necessary. The literature comparison in Table 8 is qualitative in the sense that reported conditions, core types and measurement protocols differ across sources; direct head-to-head testing under a shared protocol would be required to rank the systems unambiguously.

Against the systems listed in Table 8, the present network retained stable viscosity at 160 °C for 120 min under the tested conditions, whereas the synthetic-polymer/organic-zirconium gel of Ma et al. [15] was characterized at 200 °C and retained 147 mPa·s after 2 h, the supramolecular reinforced gel of Huang et al. [18] was likewise evaluated at 200 °C, and conventional HPG–borate fluids typically fall below 100 mPa·s under comparable high-temperature shear [1,10]; the Du et al. (2022) review range [10] brackets the broader field. The present system further yielded a residue content of 534 mg/L (0.13 wt%). Because the cited systems were tested under different protocols, these comparisons are qualitative rather than a common-benchmark ranking.

Table 8 shows that the present system combines: (i) viscosity retention (>250 mPa·s at 160 °C for 120 min), above the reported range of conventional HPG–borate systems (<100 mPa·s) and within the range of the better-performing synthetic polymer gels; (ii) core matrix damage of 17.1 ± 1.2% on the tested cores; (iii) fracture conductivity damage of

14.6% at 85 MPa, below the reported range of conventional organometallic crosslinked fluids (>25%); and (iv) on-demand complete gel breaking at 180 °C within 70 min. Because the cited systems were evaluated under different protocols, these values are indicative rather than a definitive ranking.

Table 8. Comparison of key performance indicators with representative ultra-high-temperature fracturing fluids from the literature.

Parameter	This Work	Ma et al. (2023) [15]	Huang et al. (2024) [18]	Conventional HPG–Borate [1,10]	Du et al. (2022) Review Range [10]
Base polymer/crosslinker	GHPG/organoborate	Synthetic polymer/organic Zr	Supramolecular reinforced gel (SRG)	HPG/organoboron	Various (synthetic & natural)
Test temperature (°C)	160	200	200	140–160	150–200
Viscosity after 120 min (mPa·s)	>250 (at 170 s^{-1})	147 (at 170 s^{-1}, after 2 h)	N/A (G′ ~12 Pa)	<100 (typically 50–80)	50–200 (depending on system)
Gel breaking condition	180 °C, 50 ppm APS, <70 min	200 °C, breaker, <120 min	200 °C, breaker	140 °C, APS, >120 min	–
Core matrix damage (%)	17.1 ± 1.2	16.6	~50% lower than industrial (not exact)	25–35	20–35
Fracture conductivity damage (%)	14.6 (85 MPa)	N/A	N/A	>25 (at 50 MPa)	25–40
Remarks	Simultaneous high T stability + low damage + fast break	Good T stability but higher damage potential	Ultra-low polymer loading, but damage data less direct	Poor T stability, high residue	General range for commercial fluids

2.6.7. Performance of the Weighted Formulation (14 wt% NaCl)

For ultra-deep, high-pressure reservoirs, increasing the density of the fracturing fluid can augment hydrostatic pressure and reduce wellhead pumping pressure. To evaluate the compatibility of our GHPG dynamic covalent gel with a common weighting agent, a weighted formulation was prepared by dissolving 14 wt% NaCl in the base brine before adding the polymer and other additives. The final composition was 0.55 wt% GHPG + 14 wt% NaCl + 0.5 wt% GBA1-2 + 0.5 wt% GBA1-4 + 0.5 wt% GBA1-3 + 0.15 wt% Na_2CO_3 + 0.05 wt% BA-1, with the crosslinker GBA1-1 added at 0.6 vol% immediately before testing. The pH was adjusted to 10.8 ± 0.2.

The long-term isothermal shear stability of the weighted gel was tested at 160 °C and 170 s^{-1} using the same pressurized sealed cell (2 MPa N_2). The results are presented in Figure 10. The weighted formulation maintained an apparent viscosity above 130 mPa·s for the entire 120 min test duration, meeting the typical viscosity requirement for proppant transport in deep fracturing operations. Compared with the non-weighted formulation (Figure 4), the presence of 14 wt% NaCl caused a moderate reduction in viscosity (from ≈350 mPa·s to ≈140 mPa·s after 60 min), likely due to charge screening effects that slightly reduce polymer chain expansion and crosslinking efficiency. Nevertheless, the retained viscosity remains above the industry threshold (>50 mPa·s) under the tested conditions. The weighted formulation is therefore compatible with high-salinity brines and can be used to increase fluid density for high-pressure reservoir treatments within the test window.

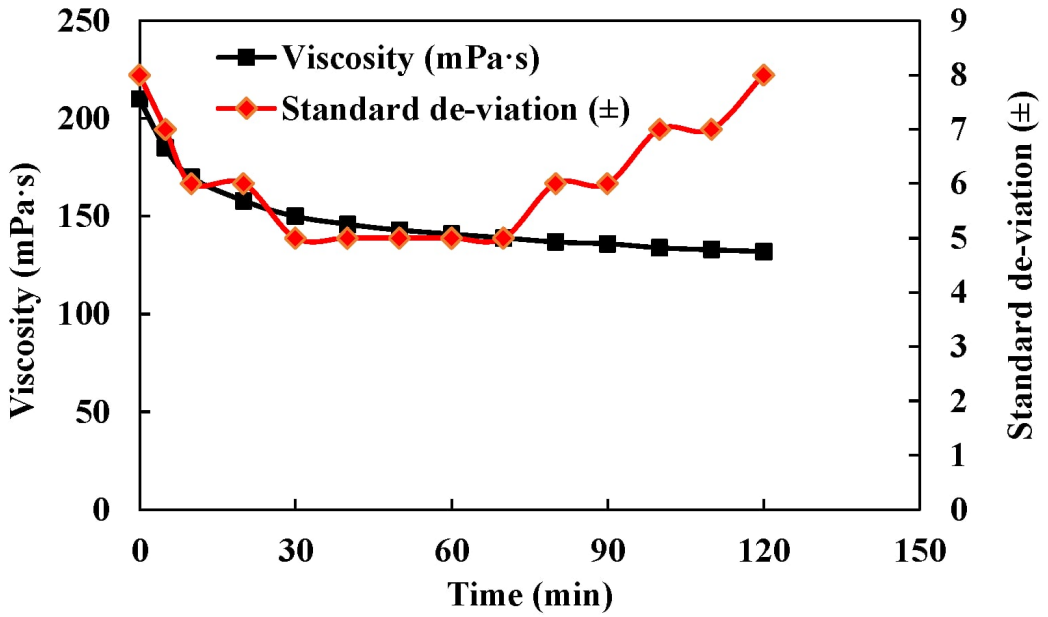


Figure 10. Viscosity-time curve of the weighted formulation (14 wt% NaCl) at 160 °C and 170 s^{-1} (n = 3, mean ± SD, shaded region). The gel maintains viscosity above 130 mPa·s for 120 min.

2.6.8. Economic Considerations

To assess the practical feasibility of the proposed GHPG dynamic covalent gel for field applications, a preliminary cost analysis was performed based on industrial raw material prices in China (2025–2026). The key components and their estimated costs are summarized in Table 9. The total material cost for the optimized formulation (0.55 wt% GHPG + 0.6 vol% GBA1-1 + functional additives) is approximately 15–20% higher than that of a conventional HPG-borate system (0.48 wt% HPG + 0.5 wt% borax + standard additives). However, the cost is significantly lower (by ≈40–50%) than that of high-performance synthetic polymer gels (e.g., polyacrylamide-zirconium systems), which require higher polymer loadings and more expensive crosslinkers. These figures are preliminary material-cost estimates based on 2025–2026 Chinese industrial raw-material list prices; they exclude service, transportation, blending equipment, chemical-additive contract pricing and field-scale bulk discounts, and should not be read as a quoted treatment cost. A full economic assessment would require supplier quotations and a per-treatment material and operating budget.

Table 9. Estimated material cost comparison for fracturing fluid systems (relative to conventional HPG-borate baseline = 1.0).

Component	Conventional HPG-Borate	This Work (GHPG)	Synthetic Polymer Gel
Base polymer	1	1.2–1.5	3.0–4.0
Crosslinker	1	1.5–2.0	2.5–3.5
Additives package	1	1.1–1.3	1.5–2.0
Total material cost (relative)	1	1.15–1.20	1.8–2.5

The total cost of a fracturing treatment must account not only for fluid materials but also for operational efficiency and post-treatment remediation. The system offers several cost-saving advantages: (i) the high thermal stability reduces the risk of premature viscosity loss and screen-out, minimizing non-productive time; (ii) the low formation damage (core damage < 19%, conductivity damage < 15%) reduces the need for costly post-fracture cleanup treatments and enhances long-term well productivity; (iii) the rapid on-demand gel

breaking at 180 °C shortens flowback time and reduces disposal costs. Therefore, despite a slightly higher upfront material cost, the GHPG-based dynamic covalent gel is economically competitive for ultra-deep, high-temperature reservoirs where conventional fluids fail to meet performance requirements. The operational and cleanup savings listed above are qualitative expectations derived from the measured rheology, damage and breakage results; they were not verified by field cost accounting, and no actual treatment expenditure was recorded in this study.

2.6.9. Implications for Heavy-Oil Reservoir Stimulation

The engineering results above carry direct implications for heavy-oil reservoir stimulation, although the present experiments were conducted on cores and fluids from high-temperature deep reservoirs. First, the sustained viscosity (>250 mPa·s after 120 min at 160 °C; >80 mPa·s after 90 min at 180 °C) supplies the proppant-carrying capacity needed to place sand across fractures in viscous-oil intervals, where high crude viscosity and heterogeneous glutenite lithology constrain sand transport and fracture geometry [5]. Second, the average core-matrix damage of 17.1 ± 1.2% and the fracture-conductivity damage of 14.64% at 85 MPa preserve the conductive capacity on which viscous oil flow toward the wellbore depends; residual polymer damage in propped fractures has been identified as a leading cause of post-fracture productivity loss across oil types [7]. Third, the broken-fluid surface tension of 27.2 $mN \cdot m^{-1}$ and the residue content of 534 $mg \cdot L^{-1}$ (0.13 wt%) favor capillary cleanup and mitigate water-block risk in water-sensitive heavy-oil matrix, while the measured compatibility with high-salinity formation water limits the risk of inorganic scaling during flowback. It should be emphasized that no crude-oil compatibility, oil–water emulsification, flowback or oil-displacement experiment was performed; the heavy-oil discussion below is a projection from the deep-reservoir results, not an experimental validation in viscous-oil cores or fluids.

Several adaptability issues must nevertheless be resolved before field use in heavy-oil reservoirs. First, oil–water interfacial tension and emulsion tendency between the broken fluid and heavy crude should be quantified, because excessive emulsification can impede oil–water separation and increase produced-water treatment cost. Second, proppant embedment and long-term conductivity under the closure-stress regimes typical of shallow-to-medium-depth heavy-oil sands, together with compatibility under cyclic steam or hot-water injection, require dedicated testing. Third, the present matrix-damage evaluation was performed at 90 °C on deep-reservoir cores; water-sensitive, clay-rich heavy-oil cores should be evaluated under representative temperature and salinity conditions. These follow-up studies would extend the percolation-controlled gel design from 160 to 180 °C deep reservoirs to the broader domain of heavy-oil stimulation.

3. Conclusions

Addressing the three core requirements for gel materials in deep reservoir fracturing stimulation at 160–180 °C—high-temperature stability, low formation damage, and controllability—this study employed a heat-resistant modified guar gum (GHPG) as the matrix. Rather than relying on empirical optimization, the study regulated the reversible crosslinked network architecture in relation to crosslinking density. The primary scientific findings and engineering outcomes are as follows:

(1) Identification of the crosslinker-concentration threshold for network transition. Under conditions of 140 °C and 170 s^{-1}, increasing the crosslinker concentration from 0.4 vol% to 0.6 vol% was found to trigger a transition in network dynamics: from a viscous, liquid-like behavior ($G'' > G'$) to an elastic, gel-like behavior ($G' > G''$ with a frequency-independent plateau modulus). This threshold concentration (0.6 vol%) marks the

onset of a cooperative, self-healing network. The network retained a viscosity above 250 mPa·s after continuous shearing at 160 °C and 170 s^{-1} for 120 min, which identifies a crosslinker-selection reference for high-temperature stable gels.

(2) Resolution of the stability–cleanliness balance via a dual-function network. By operating at the threshold concentration, the gel combines long-term structural integrity under high-temperature (160 °C) shear with complete, rapid disintegration upon triggering with 50 ppm ammonium persulfate at 180 °C (viscosity < 10 mPa·s within 70 min). This on-demand switchability addresses the tension between prolonged stability during proppant transport and rapid, clean flowback for formation protection.

(3) Temperature-dependent stability validation. The gel retained viscosity above 250 mPa·s for 120 min at 160 °C. Direct testing at 180 °C showed viscosity above 80 mPa·s for 90 min without breaker, consistent with typical fracturing treatment durations, and rapid degradation (viscosity < 10 mPa·s within 70 min) upon addition of 50 ppm APS. This combination supports applicability for deep reservoirs with bottom-hole temperatures up to 180 °C within the tested treatment window.

(4) Comprehensive engineering verification of the percolation-controlled gel. A direct control experiment with a commercial HPG–borate gel under identical conditions showed rapid viscosity decay to <100 mPa·s within 60 min at 160 °C, whereas the GHPG gel retained >250 mPa·s for 120 min. On the deep-reservoir cores and fluids tested, the system gave a drag reduction rate of 58.02% (62 mm pipe, 6.0 m^3/min, fresh water baseline), a dynamic fluid-loss coefficient as low as 3.76×10^{-4} m/$min^{0.5}$, an average core-matrix damage of 17.1 ± 1.2% (three representative core plugs), and a fracture-conductivity damage of 14.64% at 85.0 MPa closure stress. These values are better than those of conventional guar-based fluids and competitive with the best reported synthetic polymer gels, while offering on-demand rapid breakage at 180 °C. The weighted variant (14 wt% NaCl) retained above 130 mPa·s after 2 h at 160 °C, indicating adaptability for high-pressure reservoirs. All engineering results above were obtained on deep-reservoir cores and fluids; performance in heavy-oil intervals has not yet been experimentally verified. The engineering comparison reported here rests on one commercial HPG–borate control rather than multiple field-grade benchmarks; replicate numbers were three for core plugs, rheology, and conductivity, and two for the 160 °C fluid-loss test.

This work provides a gel system for fracturing in 160–180 °C ultra-deep reservoirs, and outlines a crosslinker-selection framework—centered on the 0.6 vol% threshold governing the viscous-fluid to elastic-gel transition—for rational design of high-temperature gels with programmable rheological and degradation behavior. A full percolation scaling analysis was not performed here; the frequency-sweep data provide direct evidence for the transition, and future work will address the critical exponents and a quantitative network model. The heavy-oil relevance stated below is a projected, not yet demonstrated, application: because the system exhibits low matrix damage, low residue, and conductivity protection on deep-reservoir samples, its design principles may transfer to low-damage heavy-oil fracturing. This extension remains conditional on dedicated tests of crude compatibility, oil–water interfacial tension and emulsion behavior, water-sensitive clay-rich cores, and compatibility with cyclic steam or hot-water injection [5–7].

Several limitations of the present study should be stated explicitly. First, the percolation-controlled mechanism is inferred from rheology and band-level FTIR observations; no quantitative percolation analysis or network model was fitted, and the junction-scale network morphology was not resolved by SEM, TEM, cryo-TEM, SAXS or AFM. The raw continuous FTIR traces were not retained, so only selected peak-position absorbances are reported (Figure 2); full spectral interpretation, baseline correction and deconvolution, together with

a controlled thermal-aging FTIR series and solid-state ^{11}B NMR, remain follow-up work. Second, the high-temperature fluid-loss and damage evaluations rely on a small number of replicates (two fluid-loss measurements at 160 °C; three core plugs; three conductivity replicates), so the reported spread is not statistically representative of broader reservoir samples. Third, stability was characterized within a 120 min window at 160 °C and a 90 min window at 180 °C; chemical stability beyond these times was not explored. Fourth, the commercial comparison uses a single HPG–borate benchmark. Fifth, the cost assessment is a preliminary qualitative estimate from list prices, without supplier quotations or field accounting. Sixth, heavy-oil applicability is speculative: no crude-compatibility, emulsification, flowback or oil-displacement test was performed. These gaps define the follow-up work needed before field deployment.

4. Materials and Methods

4.1. Experimental Materials

The heat-resistant modified guar gum (GHPG, industrial grade) employed in this study possesses significantly enhanced backbone rigidity owing to the incorporation of thermally stable groups (e.g., hydroxypropyl and carboxymethyl groups) onto its molecular chains, as confirmed by the manufacturer.

The functional additives used in this study are commercially available products from commercial companies. To ensure scientific reproducibility while respecting legitimate proprietary interests, Table 10 provides not only the functional description but also the chemical category, key active component(s), active content (where applicable), solvent/carrier, and supplier for each additive.

Table 10. Composition and functions of additives in the high-temperature fracturing fluid system.

Additive Type	Code	Chemical Category/Key Active Component(s)	Primary Function
Thickener	GHPG	Hydroxypropyl carboxymethyl guar gum (industrial grade, purity ≥ 92 wt%)	Viscosity enhancement; provision of crosslinking sites
Crosslinker	GBA1-1	Organoborate ester in aqueous glycol solution; active boron content: 8.5–9.2 wt%; contains organic ligand (triethanolamine) for delayed release	Construction of a dynamic borate–ester crosslinked network
Thermal stabilizer	GBA1-3	Thiourea derivative (N, N′-diethylthiourea) dissolved in isopropanol/water (1:1 *v*/*v*); active content ≥ 40 wt%	Free-radical scavenging; inhibition of thermo-oxidative degradation
Cleanup additive	GBA1-2	Nonionic fluorosurfactant (perfluoroalkyl polyethoxylated alcohol) blended with an anionic hydrocarbon surfactant (sodium dodecylbenzenesulfonate); active content ≥ 35 wt%	Reduction in surface/interfacial tension; assistance in flowback
Clay stabilizer	GBA1-4	Low-molecular-weight cationic polyquaternium-7 (acrylamide-diallyldimethylammonium chloride copolymer, Mw ~ 500,000 Da); active content ≥ 50 wt%	Inhibition of clay-mineral hydration and swelling

Table 10. *Cont.*

Additive Type	Code	Chemical Category/Key Active Component(s)	Primary Function
Biocide	BA-1	Glutaraldehyde (25 wt% aqueous solution)	Prevention of polymer biodegradation
pH regulator	Na_2CO_3	Anhydrous sodium carbonate, analytical grade (purity ≥ 99.8%)	Regulation of the alkaline environment required for the crosslinking reaction

4.2. Base Fluid Preparation

The base fluid was prepared following a standardized hydration protocol: First, the brine (2 wt% KCl in deionized water) was prepared. Under continuous mechanical stirring at 600 r/min and a constant temperature of 30 °C, the following additives were added sequentially with 5 min intervals to ensure complete dissolution: biocide BA-1 (0.05 wt%), clay stabilizer GBA1-4 (0.5 wt%), thermal stabilizer GBA1-3 (0.5 wt%), and cleanup additive GBA1-2 (0.5 wt%). Subsequently, Na_2CO_3 (0.15 wt%) was added to adjust the pH to 10.8 ± 0.2. Only after all these additives were fully dissolved and the pH was stabilized, GHPG powder (0.55 wt%) was slowly and uniformly dispersed into the solution. After stirring for 30 min, the solution was held in a 30 °C water bath for 4 h to erase the shear history and to allow the polymer chains to attain an equilibrium expanded state. This equilibration period was validated by preliminary experiments, which confirmed that the viscosity fluctuation rate was less than 2%. For crosslinked gel preparation, the crosslinker GBA1-1 (0.6 vol% unless otherwise specified) was added to the base fluid under gentle stirring (300 r/min) immediately before each rheological measurement, with the temperature maintained at 30 °C (or at the specified test temperature for high-temperature studies). This sequential addition—all additives except the crosslinker before polymer hydration, and the crosslinker immediately before testing—is critical to avoid premature borate–ester crosslinking and to ensure reproducibility.

All experiments were conducted with at least three independent replicates unless otherwise specified. Data are reported as mean ± standard deviation (SD). Statistical analyses were performed. For rheological measurements (steady shear viscosity), each reported value represents the average of three consecutive readings after the system reached a steady state, with the standard deviation typically within ±5% of the mean.

4.3. Characterization of the Base Polymer (GHPG)

To provide a quantitative basis for the observed rheological behavior, the modified guar gum (GHPG) was characterized using gel permeation chromatography with multi-angle laser light scattering (GPC-MALLS, Wyatt Technology, Dawn Heleos II, Santa Barbara, CA, USA) for molecular weight determination, and nuclear magnetic resonance (^{1}H NMR, Bruker, 400 MHz, Billerica, MA, USA) for the degree of substitution. The results are summarized in Table 11.

Table 11. Molecular characteristics of GHPG.

Parameter	Value
Mw (×10^6 Da)	2.35
PDI	1.85
DS (hydroxypropyl)	0.38
DS (carboxymethyl)	0.12
Purity (wt%)	92.5

4.4. Rheological Characterization Methods

All rheological measurements were performed using a HAAKE RS600 (Thermo Scientific HAAKE RS600, Karlsruhe, Germany) high-temperature and high-pressure rheometer equipped with a sealed, pressurized concentric-cylinder measuring cell (DG41, pressure cell P-PTD 200, Graz, Austria). Before each high-temperature test, the cell was purged with nitrogen and pressurized to 2.0 MPa (relative pressure) to completely suppress water evaporation and boiling at temperatures up to 180 °C. The sample level in the cup was visually checked through a sapphire window, and the cell was sealed with a vapor-tight cap. After each experiment, the cell was weighed to confirm that the mass loss was <0.5%, ensuring negligible evaporation.

Steady shear measurements: The viscosity was recorded under a constant shear rate of 170 s^{-1} while heating from room temperature to the target temperature at 3 °C/min. Long-term isothermal shear stability tests were conducted at the designated temperature (160 °C or 180 °C) with continuous shear at 170 s^{-1} for up to 120 min.

Dynamic oscillatory measurements: Amplitude sweeps were conducted at 140 °C and 10 rad/s over a strain range of 0.01–100% to determine the linear viscoelastic region (LVR) and yield stress. Frequency sweeps were performed within the LVR (strain 1.0%) from 0.1 to 100 rad/s. Thixotropic recovery tests (three-step) were conducted at 140 °C: Step 1—low shear (0.5% strain, 10 rad/s) for 100 s; Step 2—high shear (100% strain, 10 rad/s) for 60 s; Step 3—return to low shear for 300 s to monitor recovery.

All oscillatory measurements were performed in triplicate. The reported G′ and G″ values represent the mean of three measurements, with CV consistently below 8% for the optimal gel (0.6 vol%) and below 12% for the sub-threshold gel (0.4 vol%).

4.5. Gel-Breaking Test

At 180 °C, 50 ppm of ammonium persulfate (APS) breaker was injected into the gel after reaching steady state, and the viscosity decay was recorded under continuous shear at 170 s^{-1}.

4.6. Drag Reduction Test

Drag reduction performance was evaluated using a multi-functional flow-loop system (Loop sys) with dual-pipe loops of 62 mm and 76 mm diameters and high-precision differential-pressure transducers. For each pipe diameter, flow rate, and temperature, fresh water was circulated first to record the reference friction pressure drop; the gel was then tested under the identical loop conditions, and the drag reduction rate was computed as $DR\% = (\Delta P_{water} - \Delta P_{gel})/\Delta P_{water} \times 100\%$. Experiments were conducted at 40 °C and 80 °C with flow rates from 1.0 to 8.0 m^3/min; each test was repeated three times.

4.7. Dynamic Fluid Loss Test

Dynamic fluid-loss experiments were performed using a high-temperature, high-pressure dynamic fluid-loss apparatus. Initial screening was conducted at 90 °C and 10 MPa differential pressure for 2 h. Validation at a representative high temperature (160 °C) was performed using an upgraded HPHT system (maximum 200 °C) with a core plug from Well T2 (6953.7 m, 5.05 mD, 8.1% porosity), at 10 MPa differential pressure and 170 s^{-1} for 60 min.

4.8. Formation Damage Evaluation

Core-matrix damage: Three reservoir core plugs from the TH Oilfield were used. Dynamic displacement experiments were performed at 90 °C, 10 MPa differential pressure, and 170 s^{-1} for 2 h. Permeability was measured before and after contamination.

Fracture conductivity damage: An API standard conductivity cell was used with a proppant concentration of 10 kg/m^2. Conductivity was measured before and after gel breaking at closure stresses ranging from 25.0 to 85.0 MPa. Each measurement was performed in triplicate.

4.9. FTIR Spectroscopy

FTIR spectroscopy (Nicolet iS50, Thermo Fisher Scientific, Waltham, MA, USA) was used to identify the chemical bonding state of the borate–ester crosslinks. Samples (base fluid, 0.4 vol% gel, 0.6 vol% gel) were freeze-dried and analyzed in transmission mode over 4000–400 cm^{-1} with 4 cm^{-1} resolution. To examine the retention of junctions after high-temperature exposure, the optimal 0.6 vol% gel was also characterized after the 160 °C/120 min continuous-shear test, freeze-dried under the same protocol. Band assignments were confirmed against the GHPG base-fluid reference; a controlled thermal-aging series and solid-state ^{11}B NMR were not available in the present study and are reserved for follow-up work. The relative absorbance values summarized in Figure 2 were read at the listed peak positions on the freeze-dried samples; the full continuous transmittance traces over 4000–400 cm^{-1} were not retained in this study and could not be reprocessed.

4.10. Compatibility Test

Actual formation water from the TH Oilfield was mixed with the broken-gel fluid (viscosity < 10 mPa·s) at volumetric ratios of 2:1, 1:1, and 1:2, and observed at 70 °C for 2 h to check for precipitation or scaling.

Author Contributions: Q.W. and M.L.: writing—original draft, and writing—review and editing. J.Z.: project administration, conceptualization. H.Z.: conceptualization, funding acquisition, project administration. Y.Y.: resources, data curation, formal analysis, methodology. All authors have read and agreed to the published version of the manuscript.

Funding: This research received no external funding.

Institutional Review Board Statement: Not applicable.

Informed Consent Statement: Not applicable.

Data Availability Statement: Dataset available on request from the authors.

Acknowledgments: We would like to thank the reviewers and editors for their careful review of this manuscript.

Conflicts of Interest: Author Qi Wang was employed by the company Daqing Oilfield Kaipu Chemical Co., Ltd.; Author Hailong Zhang was employed by the company Daqing Oilfield Co., Ltd.; Author Yiming Yang was employed by the company Liaohe Oilfield Exploration and Development Research Institute; The remaining authors declare that the research was conducted in the absence of any commercial or financial relationships that could be construed as a potential conflict of interest.

References

1. Zhang, C.-B.; Wang, Y.-L.; Chen, M.-X.; Liang, S.-N.; Shi, W.-J. Research progress on high temperature resistant guar gum fracturing fluid and its damage mechanism to reservoirs. *Chem. Ind. Eng. Prog.* **2022**, *41*, 5912–5924. [CrossRef]
2. Wu, H.-M.; Zhai, X.-P.; Li, Y.-Y.; Li, J.; Li, Z.-H.; Sun, W.-T. Modified guanidine gel fracturing fluid system and performance optimization for ultra-deep and ultra-high temperature oil and gas reservoirs. *Sci. Rep.* **2024**, *14*, 20764. [CrossRef] [PubMed]
3. Li, Y.; Shen, B.; Li, S.; Chang, X.; Qu, X.; Wang, M.; Wang, S.; Chen, G. Research progress and application status of water-based fracturing fluid thickeners. *J. Dispers. Sci. Technol.* **2026**, 1–17.
4. Duan, G.-F.; Xu, Y.; Lu, Y.-J.; Shen, H.; Cai, B.; Yang, Z.-Z. Research and field test of ultra-high temperature resistant fracturing fluid system. *Drill. Fluid Complet. Fluid* **2014**, *31*, 75–77.
5. Li, Y.-P.; Zheng, B.; Wu, M.-J.; Deng, Y.-G.; Bao, L.; Fan, X.-G. Research and application of fracturing technology in ultra-low-permeability glutenite heavy-oil reservoirs in the Tuha Oilfield. *Pet. Geol. Eng.* **2018**, *32*, 96–98.

6. Dong, X.; Liu, H.; Chen, Z.; Wu, K.; Lu, N.; Zhang, Q. Enhanced oil recovery techniques for heavy oil and oilsands reservoirs after steam injection. *Appl. Energy* **2019**, *239*, 1190–1211. [CrossRef]
7. Ghosh, B.; Abdelrahim, M.; Belhaj, H. Residual damage, its consequences, and remedial measures on post-hydrofrac well productivity: Learnt lessons. *Energies* **2022**, *15*, 7194. [CrossRef]
8. Jing, X.-R.; Tan, R.; Wang, H.-K.; Li, X. A novel modified hydroxypropyl guar gum and its application in ultra-high temperature fracturing fluid. *Drill. Fluid Complet. Fluid* **2018**, *35*, 126–130.
9. Li, X.-Z.; Pan, C.; Chen, H.; Zhang, Z.; Ning, K. Preparation and performance evaluation of temperature- and salt-resistant hydrophobically associated polymer fracturing fluids. *ACS Omega* **2025**, *10*, 8281–8291. [CrossRef] [PubMed]
10. Du, J.; Liu, J.-M.; Zhao, L.-Q.; Liu, P.-L.; Chen, X.; Wang, Q.; Yu, M.-Y. Water-soluble polymers for high-temperature resistant hydraulic fracturing: A review. *J. Nat. Gas Sci. Eng.* **2022**, *104*, 104673. [CrossRef]
11. Barati, R.; Liang, J.-T. A review of fracturing fluid systems used for hydraulic fracturing of oil and gas wells. *J. Appl. Polym. Sci.* **2014**, *131*, 40735. [CrossRef]
12. Almubarak, T.; Li, L.; Ng, J.H.; Nasr-El-Din, H.; AlKhaldi, M. New insights into hydraulic fracturing fluids used for high-temperature wells. *Petroleum* **2021**, *7*, 70–79. [CrossRef]
13. Li, X.; Liu, H.; Jiang, A.; Chen, M. Research and Application of Ultra-High Temperature Organic Borate Crosslinker. *Oilfield Chem.* **2012**, *29*, 80–82.
14. Zhang, C.; Wang, Y.; Wang, Z.; Wang, H.; Liang, S.; Xu, N.; Li, D. Mechanism analysis of enhancing the temperature and shear resistance of hydroxypropyl guar gum fracturing fluid by boron-functionalized nanosilica colloidal crosslinker. *Colloids Surf. A Physicochem. Eng. Asp.* **2023**, *676*, 132154. [CrossRef]
15. Ma, Z.-F.; Zhao, M.-W.; Yang, Z.-T.; Wang, X.-Y.; Dai, C.-L. Development and gelation mechanism of ultra-high-temperature-resistant polymer gel. *Gels* **2023**, *9*, 726. [CrossRef] [PubMed]
16. Zuo, C.; Liu, P.; Du, J.; Wu, G.; Chen, X.; Liu, J. A review: Supramolecular polymers used in high-temperature fracturing fluids: Research status and prospects on the coupling relationship between molecular conformation and temperature resistance mechanism. *Geoenergy Sci. Eng.* **2025**, *247*, 213699. [CrossRef]
17. Wang, J.-R.; Wu, J.-W.; Yin, J.-R.; Xian, C.-G.; Jia, W.-F. Supramolecular fracturing fluids: Mechanism of action and research progress. *Chem. Ind. Eng. Prog.* **2024**, *43*, 5555–5568. [CrossRef]
18. Huang, Y.-P.; Yao, X.-L.; Dai, C.-L.; Wu, Y.-N.; Li, L.; Yuan, B. A Supramolecular Reinforced Gel Fracturing Fluid with Low Permeability Damage Applied in Deep Reservoir Hydraulic Fracturing. *Gels* **2023**, *10*, 2. [CrossRef] [PubMed]
19. Sánchez-Morán, H.; Ahmadi, A.; Vogler, B.; Roh, K.-H. Oxime cross-linked alginate hydrogels with tunable stress relaxation. *Biomacromolecules* **2019**, *20*, 4419–4429. [CrossRef] [PubMed]
20. Di Lorenzo, F.; Hellwig, J.; von Klitzing, R.; Seiffert, S. Macroscopic and microscopic elasticity of heterogeneous polymer gels. *ACS Macro Lett.* **2015**, *4*, 698–703. [CrossRef] [PubMed]
21. Liu, P.-L.; Zhang, L.; Xing, X.-J.; Lan, X.-T.; Li, N.-Y.; Luo, Z.-F. Characteristics of formation damage by guar-gum fracturing fluids. *Oilfield Chem.* **2014**, *31*, 334–338.
22. Guo, J.-C.; He, C.-M. Microscopic mechanism of the damage caused by gelout process of fracturing fluids. *Acta Pet. Sin.* **2012**, *33*, 1078–1082.
23. Wang, J.; Huang, Y.; Zhang, Y.; Zhou, F.; Yao, E.; Wang, R. Study of fracturing fluid on gel breaking performance and damage to fracture conductivity. *J. Pet. Sci. Eng.* **2020**, *193*, 107443. [CrossRef]
24. Wu, L.; Wang, S.; Lei, Y. Weighting performance research of ultra-high temperature guar gum fracturing fluid. *J. Chongqing Univ. Sci. Technol. (Nat. Sci. Ed.)* **2011**, *13*, 98–100, 116.
25. Lei, Q.; Xu, Y.; Yang, Z.-W.; Cai, B.; Wang, X.; Zhou, L.; Liu, H.-F.; Xu, M.-J.; Wang, L.-W.; Li, S. Progress and development directions of stimulation techniques for ultra-deep oil and gas reservoirs. *Pet. Explor. Dev.* **2021**, *48*, 221–231. [CrossRef]
26. Tan, B.; He, Z.; Fang, Y.; Zhu, L. Removal of organic pollutants in shale gas fracturing flowback and produced water: A review. *Sci. Total Environ.* **2023**, *883*, 163478. [CrossRef] [PubMed]
27. Wang, L.; Hao, Q.; Zhong, Y.; Liu, X.; Xie, Q.; Tian, X.; Qin, F. Influence of native pores on the size distribution and predictability of rock failure. *J. Rock Mech. Geotech. Eng.* **2026**, *18*, 1447–1459. [CrossRef]
28. Lei, Z.; Dou, X.; Wang, Q.; Wang, R.; Ji, D.; Chen, Z.; Xing, G. A semi-analytical model of a hydraulically fractured horizontal well with pre-Darcy flow and stimulated reservoir volume in a radial composite shale reservoir. *SPE J.* **2024**, *30*, 743–761. [CrossRef]
29. *SY/T 6376-2008*; General Technical Specifications of Fracturing Fluids. Petroleum Industry Press: Beijing, China, 2008.
30. *SY/T 5107-2016*; Performance Evaluation Method of Water-Based Fracturing Fluid. Petroleum Industry Press: Beijing, China, 2016.

Disclaimer/Publisher's Note: The statements, opinions and data contained in all publications are solely those of the individual author(s) and contributor(s) and not of MDPI and/or the editor(s). MDPI and/or the editor(s) disclaim responsibility for any injury to people or property resulting from any ideas, methods, instructions or products referred to in the content.